ORIGINAL ARTICLE

3D Synaptic Organization of the Rat CA1 and Alterations Induced by Cocaine Self-Administration

L. Blazquez-Llorca [1,2,3], M. Miguéns[4], M. Montero-Crespo[2,5], A. Selvas[1], J. Gonzalez-Soriano[3], E. Ambrosio[1,‡] and J. DeFelipe[2,5,‡]

[1]Departamento de Psicobiología, Facultad de Psicología, Universidad Nacional de Educación a Distancia (UNED), 28040 Madrid, Spain, [2]Laboratorio Cajal de Circuitos Corticales, Centro de Tecnología Biomédica, Universidad Politécnica de Madrid, 28223 Madrid, Spain, [3]Sección Departamental de Anatomía y Embriología (Veterinaria), Facultad de Veterinaria, Universidad Complutense de Madrid, 28040 Madrid, Spain, [4]Departamento de Psicología Básica I, Facultad de Psicología, Universidad Nacional de Educación a Distancia (UNED), 28040 Madrid, Spain and [5]Instituto Cajal, Consejo Superior de Investigaciones Científicas, 28002 Madrid, Spain

Address correspondence to Lidia Blazquez-Llorca, PhD, Departamento de Psicobiología, Facultad de Psicología, Universidad Nacional de Educación a Distancia (UNED), C/Juan del Rosal 10, Madrid 28040, Spain. Email: lidiblaz@ucm.es.

M. Montero-Crespo and A. Selvas have contributed equally to this work.

[‡]Cosenior authors.

Abstract

The hippocampus plays a key role in contextual conditioning and has been proposed as an important component of the cocaine addiction brain circuit. To gain knowledge about cocaine-induced alterations in this circuit, we used focused ion beam milling/scanning electron microscopy to reveal and quantify the three-dimensional synaptic organization of the neuropil of the *stratum radiatum* of the rat CA1, under normal circumstances and after cocaine-self administration (SA). Most synapses are asymmetric (excitatory), macular-shaped, and in contact with dendritic spine heads. After cocaine-SA, the size and the complexity of the shape of both asymmetric and symmetric (inhibitory) synapses increased but no changes were observed in the synaptic density. This work constitutes the first detailed report on the 3D synaptic organization in the *stratum radiatum* of the CA1 field of cocaine-SA rats. Our data contribute to the elucidation of the normal and altered synaptic organization of the hippocampus, which is crucial for better understanding the neurobiological mechanisms underlying cocaine addiction.

Key words: addiction, drug, FIB/SEM, hippocampus, synapse

Introduction

The mechanisms underlying the causes of drug addiction are not entirely known, but it is thought that the processes of learning and memory are essential and that the hippocampus plays a key role in contextual conditioning and cocaine addiction (Castilla-Ortega et al. 2016; Kutlu and Gould 2016). In fact, addiction has been considered as a type of nonadaptive learning (Milton and Everitt 2012). In this regard, the hypothesis that drugs and natural enhancers act on similar brain systems (Olsen 2011; Lüscher et al. 2020) is becoming more relevant.

Numerous studies have found that a variety of drugs of abuse produce several morphological modifications of the pyramidal neurons, including the dendritic spines, which represent the main postsynaptic target of excitatory glutamatergic synapses of the cerebral cortex (DeFelipe 2015). These changes are found in different brain regions including the frontal cortex, hippocampus, and the nucleus accumbens (e.g., Robinson and Kolb 2004; Ballesteros-Yáñez, Ambrosio, et al. 2007a; Ballesteros-Yáñez, Valverde, et al. 2007b; Russo et al. 2010; Dumitriu et al. 2012; Muñoz-Cuevas et al. 2013; Miguéns et al. 2015; Selvas et al. 2017). Previous studies in our laboratory have shown that cocaine-induced changes in the hippocampus depend on the rat strain; specifically, an increase in the dendritic spine density and the proportion of larger spines after cocaine self-administration (cocaine-self administration [SA]) in Lewis rats (Miguéns et al. 2015; Selvas et al. 2017). Several global and local processes, involving dendritic spine and synaptic reorganization (structural plasticity) occurring in a defined temporal manner, have been proposed to provide a mechanism for long-term storage of memory traces upon learning that influences behavior (Leuner and Gould 2010; Caroni et al. 2012). For this reason, dendritic spine changes, among other structural changes, might explain functional alterations—such as facilitation of long-term potentiation (LTP) or impaired LTP depotentiation in the hippocampus—as well as behavioral alterations after cocaine-SA (Thompson et al. 2002; Del Olmo et al. 2006, 2007; Fole et al. 2011, 2017; Miguéns et al. 2011). Therefore, hippocampal dendritic spines seem to be altered after cocaine consumption.

However, it has been well established via electron microscopy that dendritic shafts also form synapses and not all dendritic spines represent postsynaptic targets (Arellano et al. 2007; Bosch et al. 2016; Santuy et al. 2018a). Thus, electron microscopy with serial section reconstruction is the gold standard method for studying the normal synaptic organization and its possible alterations. Here, we used focused ion beam/scanning electron microscopy (FIB/SEM) technology to perform a three-dimensional (3D) analysis of the synaptic organization in the neuropil in the *stratum radiatum* of the CA1 region of Lewis rats—an inbred rat strain that is prone to the reinforcing effects of drugs of abuse (Cadoni 2016). This hippocampal layer receives most afferents from the Schaffer collaterals of the CA3 pyramidal neurons—a synaptic connection that has a key role in the learning-induced synaptic potentiation of the hippocampus (Whitlock 2006). We first studied the normal (control) *stratum radiatum* and then compared the results with that obtained in the *stratum radiatum* of rats after intravenous cocaine-SA. This drug consumption model is considered the best for simulating the pattern of consumption in humans (Spanagel 2017). Specifically, we studied a wide variety of synaptic structural parameters including the following: synaptic density and spatial distribution (i.e., whether synapses are arranged in a uniform, random, or clustered distribution); proportions of synapses; postsynaptic targets; as well as the shape and size of the synaptic junctions. This work constitutes the first detailed report of the 3D synaptic organization in the *stratum radiatum* of the hippocampal CA1 field of cocaine-SA rats. Our data contribute to the elucidation of the normal and altered synaptic organization of the rat hippocampus, which is crucial for better understanding the neurobiological effects of cocaine consumption.

Materials and Methods

Animals

Adult male Lewis rats ($n = 13$) were used in this study, weighing 275–350 g (Harlan Interfauna Ibérica) at the beginning of the experiments. They were housed individually in a climate-controlled room (23 °C) with a 12 h light–dark cycle (08:00–20:00 lights on) in accordance with the European Union guidelines for the care of laboratory animals (Directive 2010/63/EU) and we followed the "Principles of laboratory animal care". All the animals were experimentally naïve and, unless otherwise specified, they had free access to Purina laboratory feed (Panlab, Barcelona, Spain) and tap water.

Catheter Surgery and Cocaine Self-Administration Procedure

The surgical procedure has been described elsewhere (Miguéns et al. 2015). Briefly, rats were anaesthetized with a mixture of ketamine (40 mg/kg) and diazepam (10 mg/kg) and implanted with polyvinylchloride tubing (0.064 i.d.) into the jugular vein approximately at the level of the atrium. To evaluate the catheter patency and prevent infection, the catheters were flushed every day with 0.3 mL of an antibiotic solution (gentamicin, 0.10 mg/mL) dissolved in heparinized saline solution. Catheter patency was tested at the end of the experiments by infusing with thiopental (10 mg/kg, i.v.), and a good patency was assumed if the rat immediately lost consciousness.

Eighteen operant conditioning chambers (Coulburn Instruments, Allentown, PA, USA) with two fixed levers were used for the behavioral studies (Fig. 1). Prior to the drug self-administration phase, lever-press training was conducted. Rats were food-deprived—to facilitate the lever-pressing learning task—until they reached 95% of their free-feeding weight, and they were submitted to several free-operant daily sessions with a fixed ratio (FR) schedule of reinforcement, in which a specified number of lever-press responses of the left lever were needed to earn a food pellet, whereas presses on the right lever had no programmed consequences. The sessions started with an FR-1 schedule that was subsequently raised to FR-3 for several daily 30-min sessions until the animals developed stable lever pressing rates (rats had to obtain at least 30 pellets during one session to proceed to the next phase). The animals were then fed ad libitum, and when they had recovered their free-feeding weight, catheter surgery was performed (see above). After a postoperative recovery period (of at least 7 days), the rats were food restricted prior to initiation of the cocaine-SA—again to 95% of their original weight—and they were trained to respond to cocaine ($n = 7$) or saline ($n = 6$) infusions in daily 2-h sessions or until the rats earned 20 cocaine infusions over a period of 21 days (7 days/week). When drug/saline self-administration was initiated, rats were fed ad libitum until the end of the experiments. A microliter injection pump (Harvard 22; Harvard Apparatus) was used to deliver intravenous cocaine (1 mg/kg) or saline infusions (100 μL) over 10 s when animals pressed the left lever, while inactive lever presses were recorded but had no programmed consequences. An FR ratio of FR-1 was used in the beginning and was subsequently raised weekly, first to FR-2 and then to FR-3. During cocaine or saline infusions, a timeout period of 10 s—during which the lever was inactive—was employed in all the schedules. Following the 21 self-administration sessions,
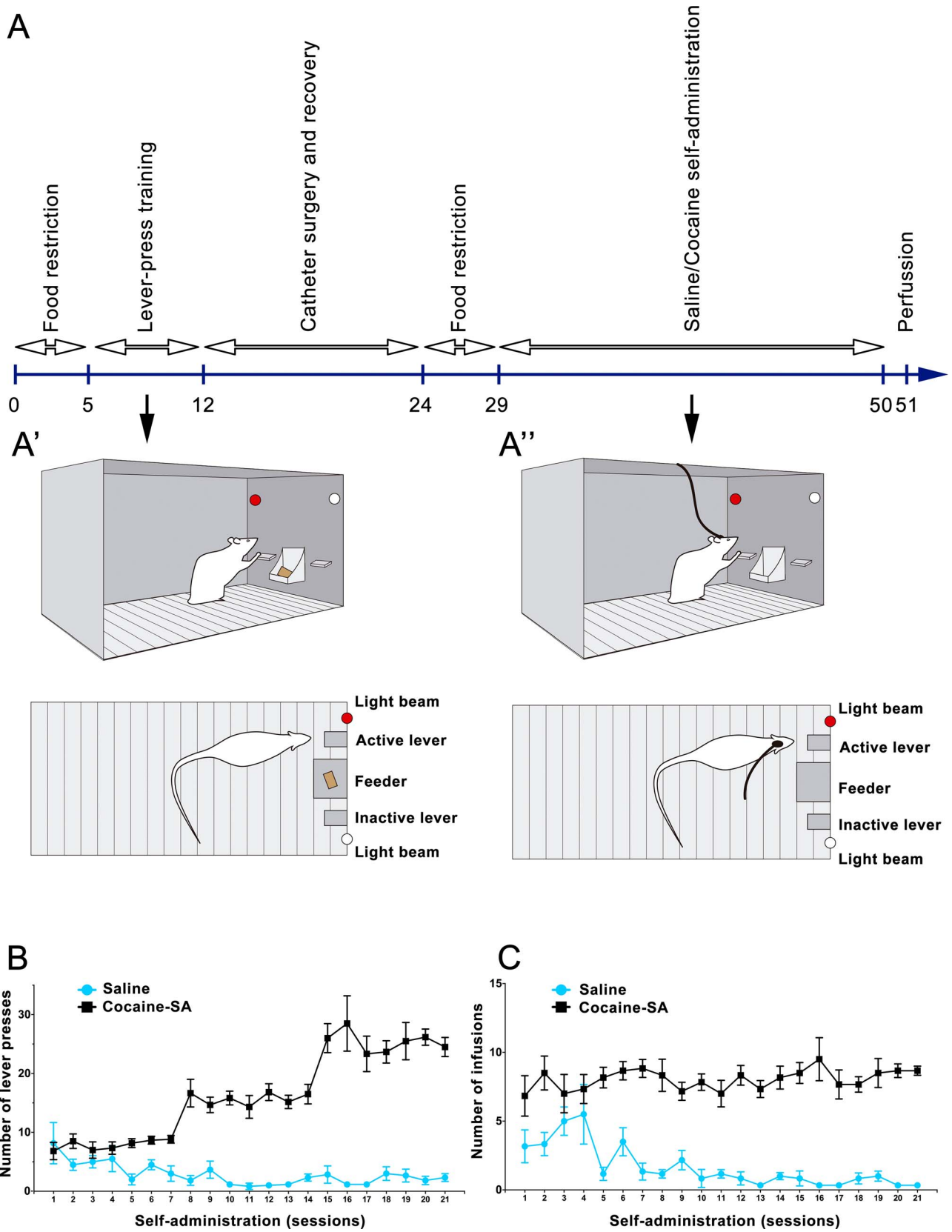
Figure 1. Self-administration procedure. (*A*) Timeline (in days) showing the different procedures performed. Following the 21 self-administration sessions, saline and cocaine-SA animals were intracardially perfused 24 h after the last session, and brains were further processed for the FIB/SEM imaging. See Materials and Methods in the main text for further information. *A'*, Shows a diagram of a 3D view (upper part) and aerial view (bottom part) of a rat carrying out the lever-press training in

saline and cocaine-SA animals were intracardially perfused, 24 h after the last session (see details below; Fig. 1).

Rats that self-administered cocaine progressively increased the number of infusions received and the number of times the lever was pressed with respect to the saline group (whose response was virtually null), reaching a stable self-administration pattern at the end of the 21 days. Animals that received cocaine showed more robust responses—number of lever presses—than saline animals during the last seven sessions under the FR-3 schedule of reinforcement (saline: 2.14 ± 1.19; cocaine-SA: 25.38 ± 4.74; $t_{10} = 11.65$, $P < 0.0001$). Total cocaine intake in self-administered animals was 161.85 ± 26.24 mg/kg (average per session: 8.03 ± 1.18 mg/kg) (Fig. 1B,C).

Tissue Preparation for Electron Microscopy

Rats were intracardially perfused with 100 mL of 1% paraformaldehyde in 0.1 M phosphate buffer (PB; pH 7.3) followed by 500 mL of 4% paraformaldehyde and 0.125% glutaraldehyde in 0.1 M PB (pH 7.3) at a flow rate of 25 mL/min. The descending aorta was clamped to preferentially restrict the flow of fixative to the upper body and accelerate perfusion of the brain. Immediately after perfusion, the brains were removed and postfixed for 6 h at room temperature in the same fixative. After postfixation, 150 μm coronal vibratome (Lancer 1000) sections were obtained.

Selected sections containing the dorsal hippocampus were washed in sodium cacodylate (Sigma, C0250-500G) buffer (0.1 M) and postfixed for 24 h in a solution containing 2% paraformaldehyde, 2.5% glutaraldehyde (TAAB, G002, UK) and 0.003% $CaCl_2$ (Sigma, C-2661-500G) in sodium cacodylate buffer (0.1 M). These sections were washed in sodium cacodylate buffer (0.1 M) and treated with 1% OsO_4 (Sigma, O5500), 0.1% ferrocyanide potassium (Probus, 23345), 0.003% $CaCl_2$, and 7% glucose in sodium cacodylate buffer (0.1 M) for 1 h at room temperature. After washing in sodium cacodylate buffer (0.1 M), the sections were stained with 2% uranyl acetate (EMS, 8473), and then dehydrated and flat-embedded in Araldite (TAAB, E021) for 48 h at 60 °C (DeFelipe and Fairén 1993). Embedded sections were glued onto a blank Araldite block and trimmed. Semithin sections (1–2 μm thickness) were obtained from the surface of the block until the region of interest was reached. Then, semithin sections were stained with 1% toluidine blue (Merck, 115930) in 1% sodium borate (Panreac, 141644). The last semithin section (which corresponds to the section immediately adjacent to the block surface) was examined under light microscope and photographed to accurately locate the region to be examined.

The blocks containing the embedded tissue were glued onto a sample stub using conductive adhesive tabs (EMS 77825-09). All the surfaces of the block—except for the one to be studied (the top surface)—were covered with silver paint (EMS 12630) to prevent charging artifacts. The stubs with the mounted blocks were then placed into a sputter coater (Emitech K575X, Quorum Emitech) and the top surface was coated with a 10–20 nm thick layer of gold/palladium to facilitate charge dissipation (Merchán-Pérez et al. 2009).

Focused Ion Beam Milling and the Acquisition of Serial Scanning Electron Microscopy Images

We used a Crossbeam 540 electron microscope (Carl Zeiss NTS GmbH) as described in Merchán-Pérez et al. (2009). This instrument combines a high-resolution field emission SEM column with a focused gallium ion beam, which can mill the sample surface, removing thin layers of material on a nanometer scale. After removing each slice (20 nm thick), the milling process was paused, and the freshly exposed surface was imaged with a 1.8-kV acceleration potential using the in-column energy selective backscattered (EsB) electron detector. The milling and imaging processes were sequentially repeated, and long series of images were acquired through a fully automated procedure, thus obtaining a stack of images that represented a 3D sample of the tissue (Merchán-Pérez et al. 2009).

This study was conducted in the neuropil—that is, avoiding the neuronal and glial somata and blood vessels—where most synaptic contacts take place (90–98%) (DeFelipe et al. 1999). Twenty-four different samples (stacks of images) were acquired in the neuropil of the *stratum radiatum*—at a distance of between 70 and 100 μm from the border of the *stratum pyramidale*—from the CA1 hippocampal region in coronal slices of 12 Lewis rats (6 from the saline group and 6 from the cocaine-SA group; 2 stacks of images were taken per animal) (Fig. 2). Image resolution in the x, y plane was 5 nm/pixel. Resolution in the z-axis (section thickness) was 20 nm and image sizes were 2048×1536 pixels. The number of sections per stack ranged from 210 to 360 (mean 265.29; total 6412 sections) (Figs 3 and 4; Supplementary Fig. 1). The total tissue volume that was imaged by FIB/SEM microscopy was 10 428 μm³ (5340 μm³ in the saline group and 5088 μm³ in the cocaine-SA group).

Tissue Shrinkage Estimation

All measurements were corrected for tissue shrinkage that occurs during osmication and plastic embedding of the vibratome sections containing the area of interest as described by Merchán-Pérez et al. (2009). We measured the surface area and thickness of the vibratome sections with Stereo Investigator (MBF Bioscience), both before and after they were processed for electron microscopy (Oorschot et al. 1991); it should be noted that the sections were already fixed and postfixed before the first measurement was made. The surface area after processing was divided by the value before processing to obtain an area shrinkage factor (p^2) of 0.97. The linear shrinkage factor for measurements in the plane of section (p) was therefore 0.99. The

an operant conditioning chamber. The light beam next to the active lever (in red) indicates that the food pellet is available. The light beam next to the inactive lever is always off. A″, Shows a diagram of a 3D view (upper part) and aerial view (bottom part) of a rat carrying out the saline/cocaine self-administration procedure in an operant conditioning chamber. The light beam next to the active lever (in red) indicates that the saline/cocaine is available. The light beam next to the inactive lever is always off. (B, C) Graphs showing the average number of lever presses (B) and number of infusions (C) per session. The number of lever-presses with an FR-1 schedule (days 1–7), FR-2 schedule (days 8–14), and FR-3 schedule (days 15–21) is shown in B. To determine whether the cocaine-SA had an effect on the number of lever-presses, we conducted a 2-way ANOVA with a between-subjects factor ("treatment": cocaine vs. saline) and a within-subjects factor ("administration session": sessions 1–21). This revealed a significant interaction between treatment × session ($F_{20,200} = 15.72$, $P < 0.0001$), indicating that the rats that received cocaine carried out more lever presses from day 1 (6.83 ± 1.470; mean ± SEM) to day 21 (24.50 ± 1.628; mean ± SEM). Cocaine self-administered animals (black line) showed a higher number of infusions than the saline group (blue line). The 2-way ANOVA revealed a treatment × session significant interaction effect ($F_{20,200} = 3.114$, $P < 0.0001$), and an effect of treatment ($F_{1,10} = 144.5$, $P < 0.0001$). See Materials and Methods in the main text for further information.
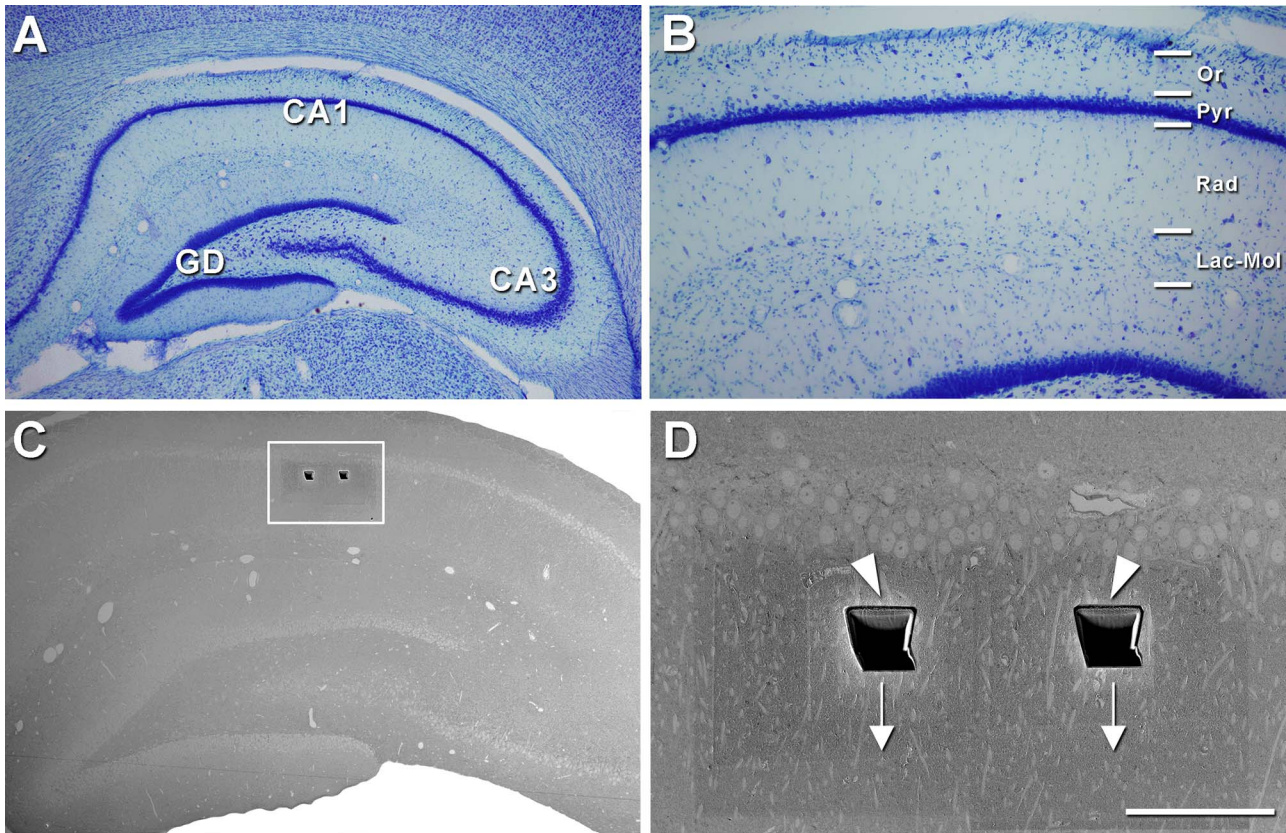
Figure 2. FIB/SEM imaging in the *stratum radiatum* of the rat CA1. (A) Low-magnification photomicrograph of a coronal Nissl-stained brain section containing the hippocampus (CA1 and CA3: *Cornu ammonis* 1 and 3, GD: dentate gyrus). (B) Higher magnification of the CA1 regions showing the layers (Or: *stratum oriens*, Pyr: *stratum pyramidale*, Rad: *stratum radiatum*, Lac-Mol: *stratum lacunosum-moleculare*). (C) Image taken with the SEM from the surface of the block containing the hippocampus to be analyzed. Rectangle surrounds the region shown in *D*. (D) Image taken with the SEM showing—at higher magnification—the *stratum pyramidale* and the trenches (arrowheads) opened with the FIB in the *stratum radiatum* to acquire the FIB/SEM serial images. Arrows indicate the direction of the FIB/SEM imaging. Scale bar in *D* corresponds to: 1 mm in (A) 412 μm in (B) 625 μm in (C) 100 μm in D.

shrinkage factor in the z-axis was 0.96. All parameters measured were corrected to obtain an estimate of the preprocessing values. Corrected and uncorrected data for each parameter are shown in Table 1.

Due to technical constraints, we did not evaluate the effect of the perfusion of the brain with paraformaldehyde and glutaraldehyde and postfixation in the same fixative. Aldehyde fixation is thought to induce tissue shrinkage, thereby biasing structural quantification (see Korogod et al. 2015; Yakoubi et al. 2019). A direct comparison of structural parameters obtained from either aldehyde or cryo-fixed and substituted tissue samples (Korogod et al. 2015) showed differences in cortical thickness (~16% larger in cryo-fixed material), volume of extracellular space (~6-fold larger in cryo-fixed material), synaptic density (~38% lower in cryo-fixed material), and the volume fraction of neuropil occupied by astrocytes (~50% lower in cryo-fixed material), but no significant differences in neuronal structures such as the volume fraction of neuropil occupied by axons and dendrites, or vesicle diameter. However, large-scale preservation for ultrastructural analysis will continue to rely on chemical fixation approaches, due to the limited preservation of the ultrastructure in cryo-fixed material, as stated in Korogod et al. (2015). Many recent studies from laboratories that are renowned in the study of synapses at the electron microscope level (using aldehydes as fixatives) do not apply any shrinkage correction factor, or—if it is applied—an explanation is not provided (e.g.,

Dufour et al. 2015; Kasthuri et al. 2015; Luebke et al. 2015; Bromer et al. 2018; Calì et al. 2018; Kulik et al. 2019; Motta et al. 2019; Yakoubi et al. 2019).

3D Analysis of Synapses

Classification of Synapses, Identification of the Postsynaptic Target, the Synaptic Shape, and Morphological Measurements
Stacks of images obtained by the FIB/SEM were analyzed using EspINA software (EspINA Interactive Neuron Analyzer, 2.8.2; https://cajalbbp.es/espina/), which allows the segmentation of synapses in stacks of serial sections (for a detailed description of the segmentation algorithm, see Morales et al. 2011; Fig. 5). As previously discussed in Merchán-Pérez et al. (2009), there is a consensus for classifying cortical synapses into asymmetric (AS) (or type I) and symmetric (SS) (or type II) synapses. The main characteristic distinguishing these synapses is the prominent or thin postsynaptic density (PSD), respectively. Nevertheless, in single sections, the synaptic cleft and the pre- and post-synaptic densities are often blurred if the plane of the section does not pass at right angles to the synaptic junction. Since the software EspINA allows navigation through the stack of images, it was possible for the user to unambiguously identify every synapse as AS or SS based on the thickness of the PSD. Synapses with prominent PSDs are classified as AS, while those with thin PSDs are classified as SS (Figs 3 and 4; Supplementary Fig. 1).
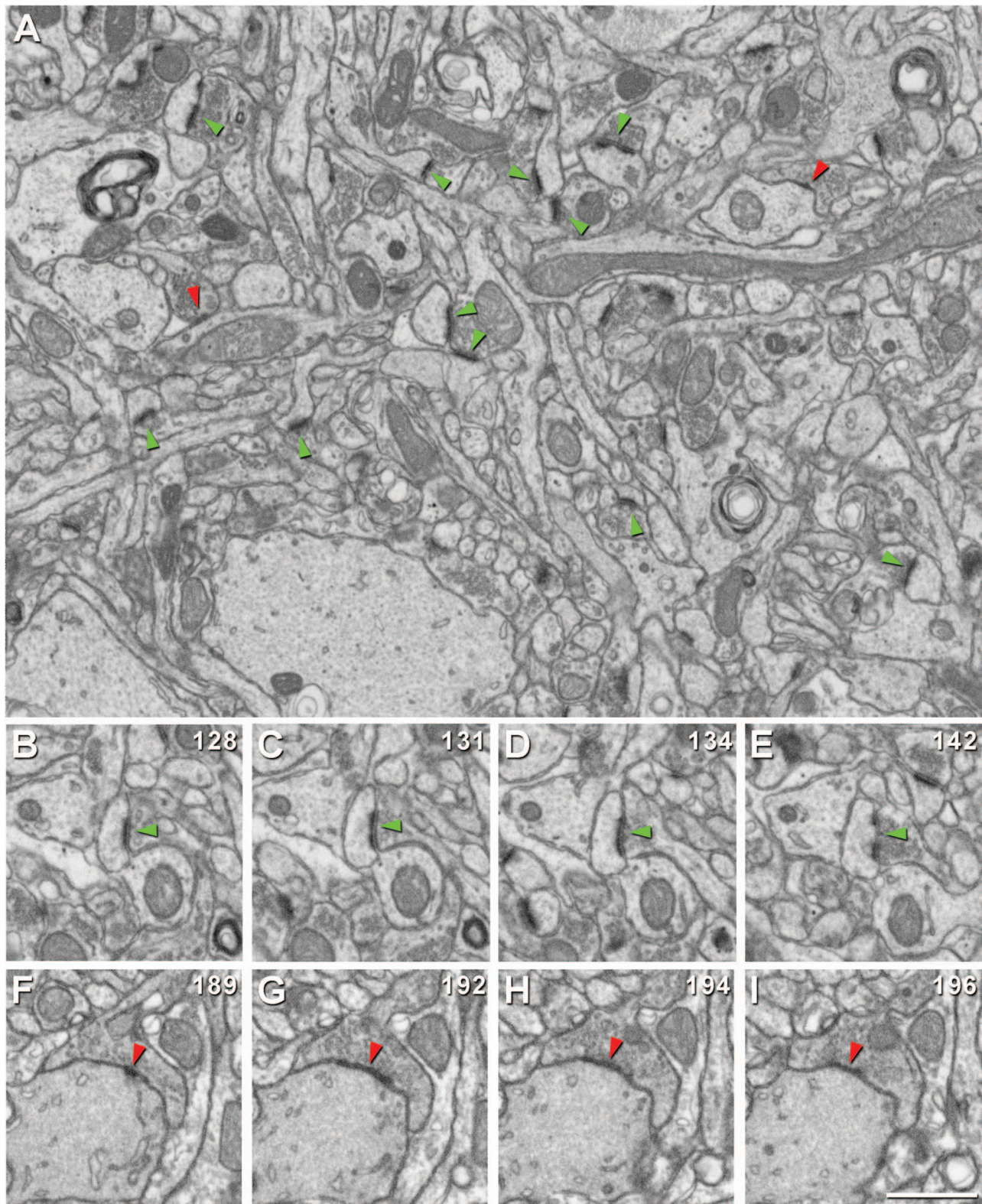
Figure 3. FIB/SEM images in the *stratum radiatum* of the rat CA1. (A) Example of an FIB/SEM image from a stack of images. Some AS and SS synapses have been pointed out (green and red arrowheads, respectively). (B–E) Same AS in different sections from the stack of images. (F–I) Same SS in different sections from the stack of images. The number of the section is indicated in the top right-hand corner of each section. Scale bar in *I* corresponds to: 0.95 μm in A, 0.79 μm in *B–I*.
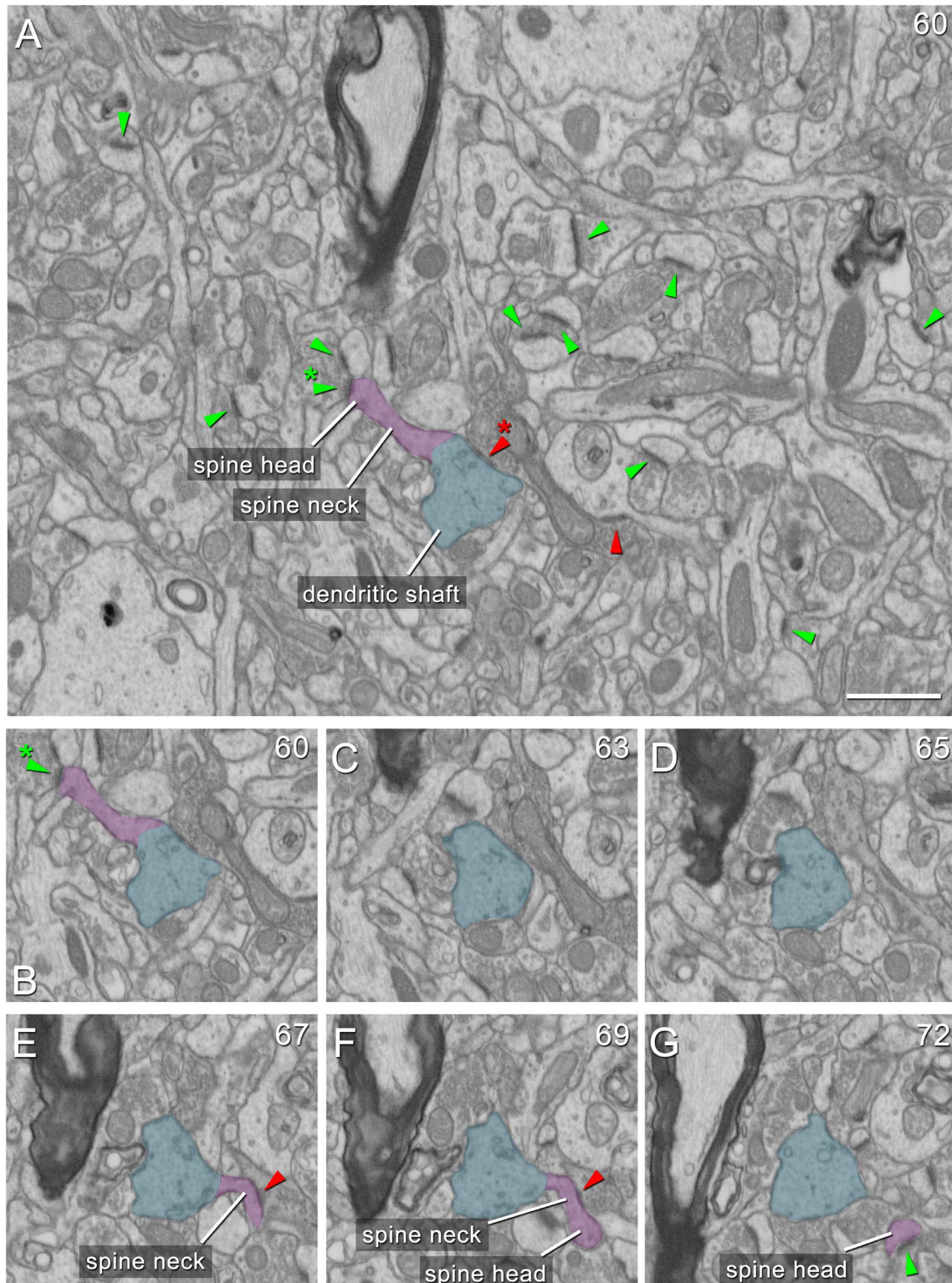
Figure 4. Differentiation of asymmetric and symmetric synapses and postsynaptic targets in the FIB/SEM stack of images. (A) Example of an FIB/SEM image from a stack of images. Some AS and SS synapses have been pointed out (green and red arrowheads, respectively). In addition, a spiny dendritic shaft (blue) with a dendritic spine (purple) emerging from the shaft is shown. The neck and the head of the spine have been indicated. An SS on the dendritic shaft is pointed out with a red arrowhead. An axospinous AS (green arrowhead) is established on the head of the spine. (B) A crop from A showing the same dendritic shaft and spine. (C–G) Serial FIB/SEM images from the same cropped area in B to illustrate another dendritic spine emerging from the same shaft, by following up the stack of images. Note that in some images only the spine neck is observed (E), while in others it is possible to see only the spine head with no connection between it and the dendritic shaft (G). An SS on the spine neck (red arrowhead) is observed in E and F. An axospinous AS (green arrowhead) is observed in G. The number of the section is indicated in the top right-hand corner of each section. Scale bar in A corresponds to: 1.3 µm in A, 1.4 µm in B–G.

Table 1 Data from the ultrastructural analysis of synapses in the neuropil of the *stratum radiatum* of the rat CA1 field in the saline and the cocaine-SA group

	Saline	Cocaine-SA
No. synapses	10 990	9069
No. AS	10 561	8756
No. SS	429	313
% AS	96.25	96.54
% SS	3.75	3.46
CF volume (μm^3)	4239 (4427)	3774 (3941)
No. synapses/μm^3 (mean $\pm$ SEM)	2.52 $\pm$ 0.13 (2.63 $\pm$ 0.14)	2.29 $\pm$ 0.13 (2.39 $\pm$ 0.14)
No. AS/μm^3 (mean $\pm$ SEM)	2.42 $\pm$ 0.13 (2.53 $\pm$ 0.13)	2.21 $\pm$ 0.13 (2.31 $\pm$ 0.14)
No. SS/μm^3 (mean $\pm$ SEM)	0.094 $\pm$ 0.008 (0.099 $\pm$ 0.009)	0.078 $\pm$ 0.003 (0.081 $\pm$ 0.003)
Area of AS SAS (nm^2; mean $\pm$ SEM)	42 022 $\pm$ 2310 (40 206 $\pm$ 2422)	48 916 $\pm$ 3249 (47 522 $\pm$ 3156)
Area of SS SAS (nm^2; mean $\pm$ SEM)	67 972 $\pm$ 6025 (66 256 $\pm$ 5825)	90 738 $\pm$ 9799 (88 153 $\pm$ 9520)
Perimeter of AS SAS (nm; mean $\pm$ SEM)	996 $\pm$ 32 (981 $\pm$ 32)	1077 $\pm$ 34 (1062 $\pm$ 34)
Perimeter of SS SAS (nm; mean $\pm$ SEM)	1507 $\pm$ 81 (1485 $\pm$ 80)	1916 $\pm$ 153 (1888 $\pm$ 151)
Curvature of AS SAS (mean $\pm$ SEM)	0.0037 $\pm$ 0.0003	0.0034 $\pm$ 0.0002
Curvature of SS SAS (mean $\pm$ SEM)	0.0028 $\pm$ 0.0004	0.0031 $\pm$ 0.0007
Volume fraction of mitochondria (%; mean $\pm$ SEM)	7.31 $\pm$ 0.20	7.49 $\pm$ 0.23

Notes: AS, asymmetric synapses; CA, *cornu Ammonis*; CF, counting frame; No., number; SA, self-administration; SAS, synaptic apposition surface; SEM, standard error of the mean; SS, symmetric synapses. Data in parentheses are not corrected with the shrinkage factor

If a particular synapse was ambiguous (which occurred rarely), additional synapses of the same axon were found and analyzed until a clear assignment could be made. As previously mentioned in Santuy et al. (2018a), this distinction is important because, in general, AS are excitatory (glutamatergic) and SS are inhibitory (GABAergic) (Ascoli et al. 2008). Although it has been described that terminals that establish AS and SS can synthesize neurotransmitters other than glutamate and GABA, respectively, such as acetylcholine, serotonin, noradrenaline, or dopamine, a large proportion of these axonal systems are nonsynaptic (DeFelipe and Jones 1988; Beaulieu and Somogyi 1990; Descarries and Mechawar 2000). Therefore, it follows that AS and SS that use acetylcholine, serotonin, noradrenaline, or dopamine must represent a very small proportion of the total number of AS and SS.

EspINA provides the number of synapses within an unbiased 3D counting frame (CF) of known volume, so the local density of synapses could be established (see Merchán-Pérez et al. 2009 for details). As previously described (Morales et al. 2011), this unbiased CF is a regular rectangular prism bounded by three acceptance planes and three exclusion planes (Howard and Reed 2005; Fig. 5C). All synapses within the CF or intersecting any of the acceptance planes are counted, while any synapse outside the CF or intersecting any of the exclusion planes is not. The position of the six planes is automatically optimized by the software to ensure that none of the synapses included in the analysis is incomplete (i.e., touching a border of the FIB/SEM stack of images). The total tissue volume analyzed, once the CF was applied, was 8013 μm^3 (4239 μm^3 in the saline group and 3774 μm^3 in the cocaine-SA group).

The 3D segmentation of synaptic junctions includes both the presynaptic density (active zone; AZ) and the PSD. Since the AZ and the PSD are located face to face, their surface areas are very similar (correlation coefficients over 0.97; Schikorski and Stevens 1997, 1999). Thus, they can be simplified to a single surface and represented as the surface of apposition between the AZ and the PSD. This surface can be extracted from the 3D segmented synaptic junction (Morales et al. 2013). For the sake

of clarity, we have referred to this surface as the synaptic apposition surface (SAS) (Fig. 5D–I). The SAS areas and perimeters of each synaptic junction were extracted with EspINA software to study morphological parameters regarding synapses. This software also permits the quantitation of the curvature of the synapses as it adapts to the curvature of the synaptic junction. Specifically, curvature measurements are calculated as 1 minus the ratio between the projected area of the SAS and the area of the SAS (Morales et al. 2011). This measurement would be 0 in a flat SAS and would increase to a maximum value of 1 as the SAS curvature increases.

Additionally, based on the postsynaptic targets, synapses were further classified as axospinous synapses (synapses on dendritic spines) and axodendritic synapses (synapses on dendritic shafts). In the case of axospinous synapses, they were further subdivided into axospinous synapses on the head or on the neck of the spine. For axodendritic synapses, dendritic shafts were further classified as spiny (when dendritic spines could be observed emerging from the shaft) or aspiny (Supplementary Fig. 1). As described in Santuy et al. (2018a), only clearly identifiable postsynaptic elements were quantified (i.e., elements that were unambiguously visually identified from navigating through the stack of images; Fig. 4) and a tag with the corresponding postsynaptic target was added to each synapse. We also recorded whether a spine was receiving a single synapse or more than one synapse (multiple synapses) on its head once the CF had been applied. Thus, the proportion of dually innervated spines with AS + AS or AS + SS was calculated regarding only the synapses identified within the CF.

Finally, synapses were classified—according to the shape of their synaptic junction—into four categories, as described elsewhere (Santuy et al. 2018b). Synapses with a flat, disk-shaped PSD were classified as macular. A second category was established by the presence of an indentation in the perimeter (horseshoe-shaped synapses). Synaptic junctions with one or more holes in the PSD were referred to as perforated. Synaptic junctions with two or more physically discontinuous PSDs were categorized as fragmented (Fig. 5F–I, see Fig. 8A). Throughout the
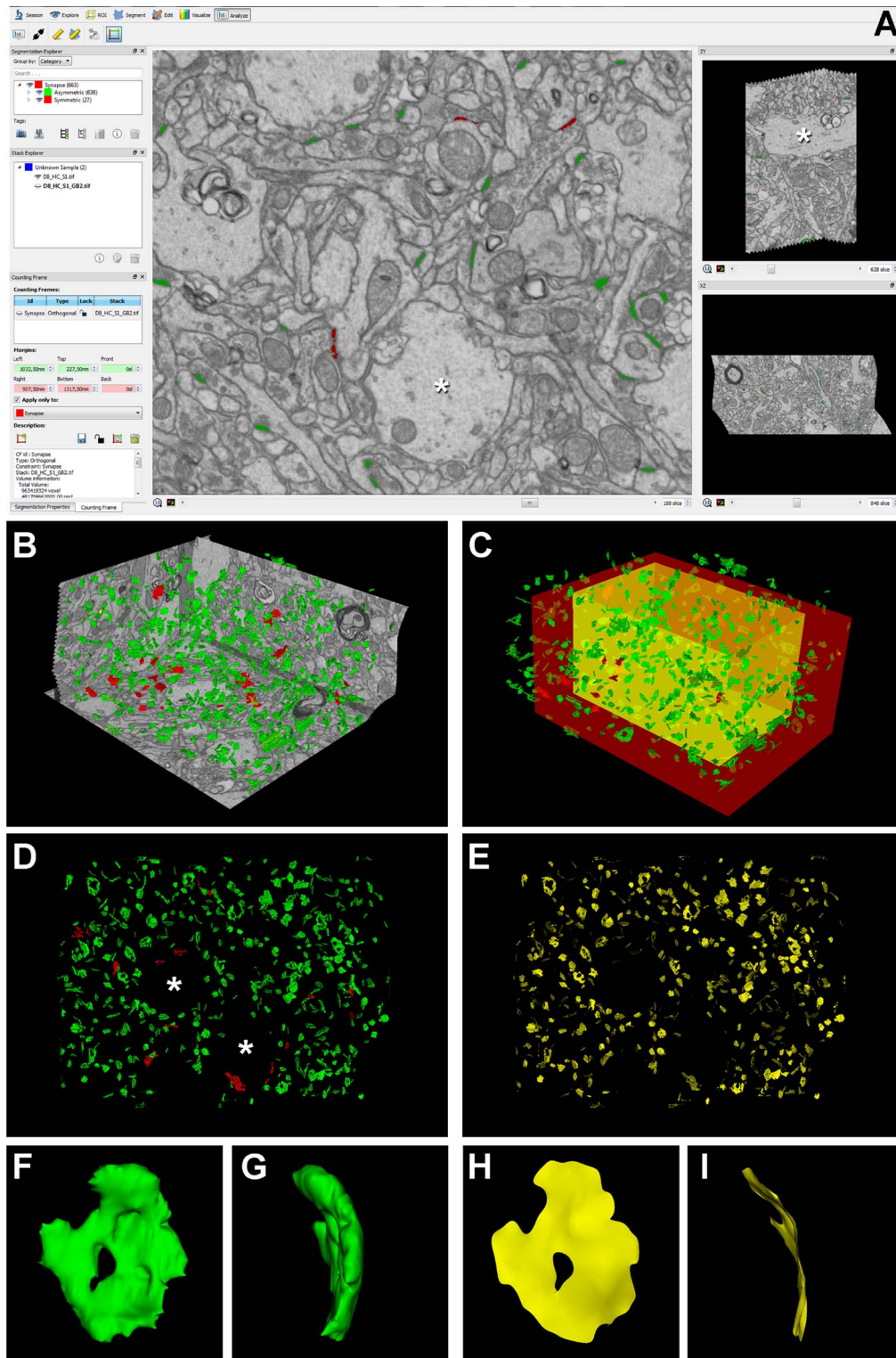
Figure 5. Analysis of the FIB/SEM stack of images with EspINA software. (A) Screenshot from the EspINA software interface, which allows visualization of the image stacks and permits the identification and 3D reconstruction of all synapses in all spatial plans (XY, XZ, and YZ). Asterisks point out large apical dendrites observed in the FIB/SEM stack of images: in the center, a coronally cut apical dendrite is observed and, on the right, the same dendrite in a lateral view, showing its elongated shape. (B) 3D view of the three orthogonal planes and the 3D reconstruction of segmented synapses. (C) Synapses are represented together with the CF. Only synapses inside the inclusion volume of the CF are analyzed to ensure that all of them are complete (the exclusion area is shown in red; the inclusion area in yellow). (D) Frontal 3D view of reconstructed synapses. Asterisks point out two spaces free of synapses due to the presence of large apical dendrites in the stack of images. (E) Same frontal 3D view as in D but showing the SAS extracted from each reconstructed synapse. (F, G) Two different 3D views of the same reconstructed asymmetric synapse. (H, I) Same 3D views as in F, G, respectively, but showing the SAS extracted from the reconstructed synapse. Note the presence of a perforation in this synapse. Asymmetric synapses are colored in green and symmetric synapses in red.

text, we also refer to the group of horseshoe-shaped, perforated, and fragmented synapses as synapses with complex shapes.

Spatial Distribution Analysis of Synapses

To analyze the spatial distribution of synapses, spatial point pattern analysis was performed as described elsewhere (Merchán-Pérez et al. 2009; Anton-Sanchez et al. 2014). Briefly, we recorded the spatial coordinates of the centers of gravity or centroids of synaptic junctions in 24 samples obtained from the corresponding stacks of serial sections. We then calculated the F, G, and K functions to compare the actual position of centroids of synapses with the complete spatial randomness (CSR) model, or homogeneous spatial Poisson point process, where a point is equally likely to occur at any location within a given volume. The F function or empty-space function is the cumulative plot of distances between a regular grid of points and the closest sample points. The G function is the cumulative plot of distances from each point to its nearest neighbor. The K function is given by the number of points within a sphere of increasing radius, centered on each sample point (Illian et al. 2008; Gaetan and Guyon 2009). We used R software (https://www.r-project.org/) and spatstat package (Baddeley and Turner 2005; Baddeley et al. 2015) (http://spatstat.org/) for the calculations. A sample was considered to be compatible with the CSR model when the observed F, G, and K functions lay within the envelope generated by 99 simulations of the CSR model (see Fig. 6C). Deviations in G functions occur because synaptic junctions cannot overlap, and thus the minimum intersynaptic distances (measured between their centroids) must be limited by the sizes of the synaptic junctions themselves (see Fig. 6C and Merchán-Pérez et al. 2014).

Estimation of the Volume Fraction Occupied by Mitochondria

We used the Cavalieri method (Gundersen et al. 1988) to estimate the volume fraction of neuropil occupied by mitochondria in the stacks of FIB/SEM images. We used Image J Stereology Toolset (Mironov 2017) to analyze the 24 stacks of images described above. A grid with an area per point of 0.25 μm^2 was used. The estimations were made in every 10th section of each stack ($z = 200$ nm). A total of 624 sections were analyzed. The parameters used for the Cavalieri method (grid size and number of sections) were chosen based on a pilot study (Broskey et al. 2013). Coefficients of error and variation were calculated to ensure the reliability of the measurements (Howard and Reed 2005).

Statistical Analysis

Statistical analysis of the data was carried out using GraphPad Prism statistical package (Prism 7.00 for Windows, GraphPad Software Inc., USA), SPSS software (IBM SPSS Statistics for Windows, Version 24.0. Armonk, NY: IBM Corp) and R Project software (R 3.5.1; Bell Laboratories, NJ, USA; http://www.R-project.org). Unpaired parametric tests were used when normality and homoscedasticity criteria were met; otherwise, equivalent nonparametric tests were used. Differences in 1) the mean synaptic density, 2) the mean SAS area, SAS perimeter, or SAS curvature, and 3) the mean volume fraction occupied by mitochondria were analyzed by performing a two-sided, t-Student test or one-way analysis of variance (ANOVA) (with Bonferroni correction posthoc tests). When necessary, the equivalent nonparametric Mann–Whitney U (MW) test or Kruskal–Wallis (KW) test (with MW pairwise comparisons) was used, respectively. In addition,

when comparing mean values, the "n" per group corresponds to the number of animals. Frequency distributions were analyzed using Kolmogorov–Smirnov (KS) nonparametric tests. To perform statistical comparisons of AS and SS, postsynaptic targets and synaptic shapes proportions, χ^2 test was used for contingency tables. In some χ^2 statistical analyses, we firstly performed an "omnibus test" based on 2×4 contingency tables. To further investigate the specific cells driving the significance of the χ^2 test, a partitioning procedure was applied to create 2×2 contingency tables (Sharpe 2015). Note that due to the large sample size of synapses analyzed—especially for AS whose numbers were in the thousands—statistical differences in KS and χ^2 tests should be carefully considered when $P > 0.001$ to avoid the overestimation of differences.

Results

We have analyzed the synaptic organization of the *stratum radiatum* of the CA1 hippocampal region of control Lewis rats (saline group) in serial sections and evaluated possible differences in this synaptic organization after cocaine-SA.

Synaptic Density and Ratio of Asymmetric and Symmetric Synapses

After discarding incomplete and excluded synapses via the CF, a total of 19 317 synapses were analyzed, of which 10 990 synapses were from the saline group (10 561 AS and 429 SS; total tissue volume analyzed: 4239 μm^3, Table 1) and 9069 from the cocaine-SA group (8756 AS and 313 SS; total tissue volume analyzed: 3774 μm^3, Table 1). The number of synapses per unit volume (synaptic density) was calculated by dividing the total number of synapses by the volume of the CF.

The synaptic density (including both AS and SS) in the saline group was 2.52 synapses/μm^3, comprising 2.42 and 0.094 synapses/μm^3 for AS and SS, respectively; that is, the ratio of AS to SS was 96.25:3.75 (Fig. 6A,B; Table 1).

No differences were found after cocaine-SA regarding synaptic density (including both AS and SS) (2.29 synapses/μm^3 in cocaine-SA group; $t_{10} = 1.208$, $P = 0.255$; Fig. 6A; Table 1) or when analyzing the densities of AS and SS separately (AS: 2.21 synapses/μm^3 in cocaine-SA group, $t_{10} = 1.145$, $P = 0.279$; and SS: 0.078 synapses/μm^3 in cocaine-SA group, $t_{10} = 1.870$, $P = 0.091$; Table 1). The ratio of AS to SS was also unaltered after cocaine-SA (96.54:3.46 in cocaine-SA group, $\chi^2 = 2.853$, $P = 0.091$; Fig. 6B; Table 1).

Synaptic Spatial Distribution

An analysis of the spatial distribution of synapses was performed for all synapses (AS and SS together). Our results indicate that the spatial organization of synapses in the neuropil of the *stratum radiatum* is nearly random, since only slight deviations from the CSR model were found (Fig. 6C). No significant differences were observed in the spatial distribution of synapses between the saline and the cocaine-SA group (Fig. 6C).

Distribution of Postsynaptic Targets

Two main postsynaptic targets were considered (Fig. 4): dendritic spines (axospinous synapses) and dendritic shafts (axodendritic synapses). In the case of axospinous synapses, the exact location of the synaptic contact was determined (i.e., the head or
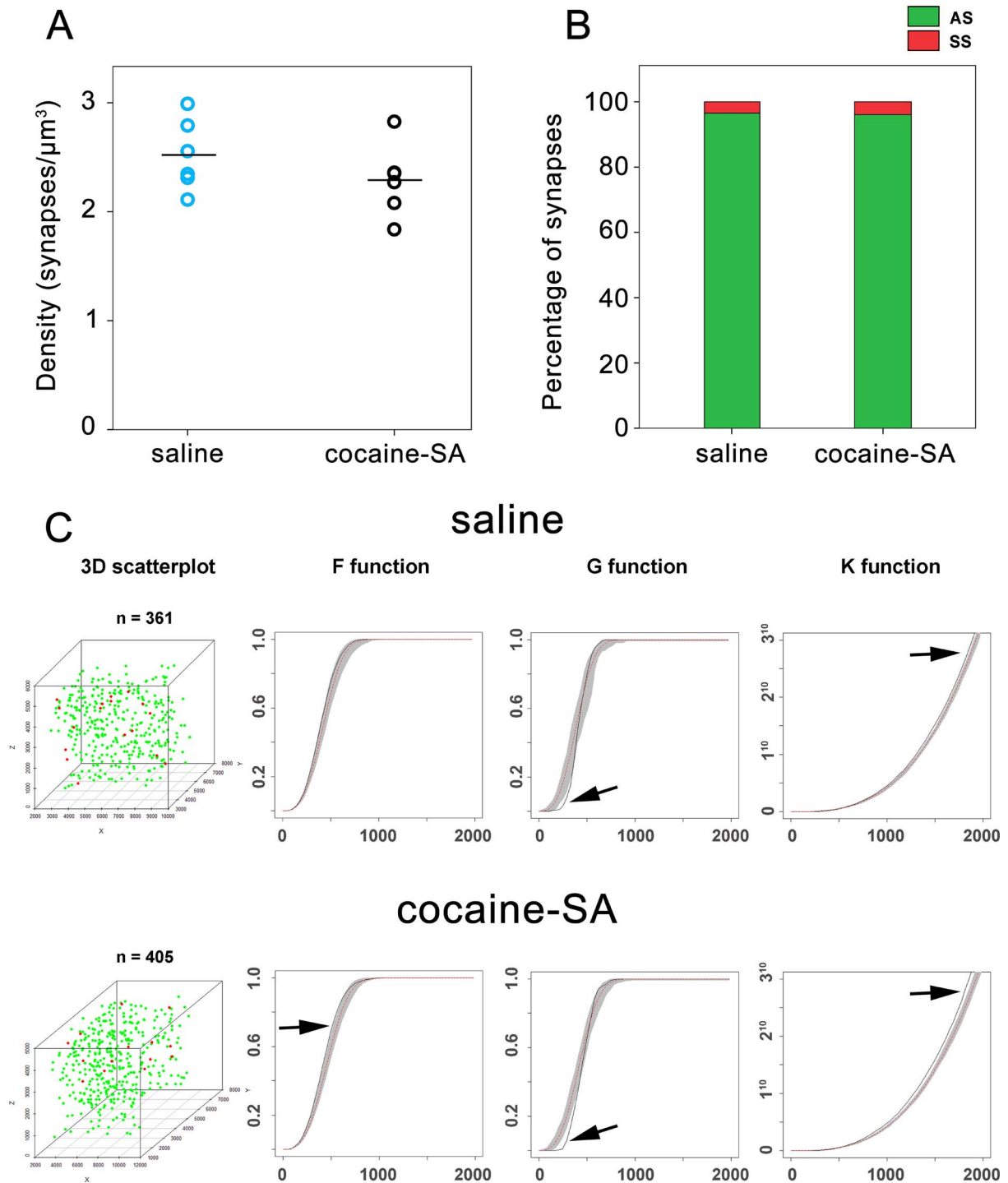
Figure 6. Synaptic density, proportions, and spatial distribution in the *stratum radiatum* of the rat CA1 in the saline and the cocaine-SA groups. (A) Graph showing the mean synaptic density (synapses/μm^3) of all synapses. Each circle corresponds to the mean synaptic density value in each animal ($n=6$ in the saline group and $n=6$ in the cocaine-SA group). (B) Graph showing the percentage of AS and SS synapses in the saline and the cocaine-SA group. (C) Example of the synaptic spatial distribution analysis in two samples—one from the saline group and the other from the cocaine-SA group (upper and bottom rows, respectively). For each synapse, we recorded the spatial positions of the center of gravity or centroid of the synaptic junction, as represented in the 3D scatterplots of the leftmost column (with the number of synapses analyzed shown above each of the two scatterplots; AS in green and SS in red). Three spatial statistical functions (F, G and K) were calculated for each group of synapses in each sample. In each graph, the function corresponding to the actual sample is represented by a black line. The theoretical homogeneous Poisson distribution or CSR is represented as a red discontinuous trace, and the gray envelope is generated by 99 simulations of the CSR model. The spatial distribution of all synapses was nearly random, since all three functions lay within the simulated envelopes or deviated only slightly (arrows). Deviations in G functions occur because synaptic junctions cannot overlap, and thus the minimum intersynaptic distances (measured between their centroids) must be limited by the sizes of synaptic junctions themselves. Deviations in F and K functions can be due to the presence of large apical dendrites in this layer of CA1 that leave spaces free of synapses (see Fig. 5A,D). No differences were observed in the synaptic density ($t_{10}=1.208$, $P=0.255$), the proportion of AS or SS ($\chi^2=2.853$, $P=0.091$), or the spatial distribution of synapses after cocaine-SA. SA: self-administration.

neck of the dendritic spine). For axodendritic synapses, dendritic shafts were further classified as spiny (when dendritic spines could be observed emerging from the shaft) or aspiny (Supplementary Fig. 1). Only synapses whose postsynaptic target was clearly identifiable after navigation through the stack of images (saline group: $n = 5029$; AS = 4818, SS = 211; cocaine-SA group: $n = 4708$; AS = 4535, SS = 173) were considered for analysis (Supplementary Table 1).

Saline Group
Total synaptic population. Most synapses (AS+SS) were established on dendritic spines—especially on the head—($n = 4775$; 94.94%) rather than on dendritic shafts ($n = 254$; 5.06%) ($\chi^2 = 4064.315$, $P = 0.000$). Synapses (AS+SS) on spiny shafts were more abundant than synapses on aspiny shafts (4.11% and 0.95%, respectively, $\chi^2 = 8599.176$, $P = 0.000$) (Fig. 7A).

As a whole, axospinous AS were clearly the most abundant type of synapse ($n = 4738$; 94.21%), followed by axodendritic SS ($n = 174$; 3.48%), axodendritic AS ($n = 80$; 1.58%), and axospinous SS ($n = 37$; 0.73%) (Fig. 7A).

Postsynaptic preference of AS and SS. Most AS were established on dendritic spines ($n = 4738$, 98.34%; Fig. 7E, Supplementary Table 1) and almost exclusively on the head of the spines (99.98%; Fig. 7B). The remaining AS were established on dendritic shafts ($n = 80$, 1.66%–52.5% of which were on spiny dendritic shafts and 47.5% on aspiny shafts; Fig. 7B,E, Supplementary Table 1). By contrast, most SS were axodendritic ($n = 174$, 82.47%; Fig. 7E, Supplementary Table 1) and had a clear preference for spiny shafts versus (vs.) aspiny shafts (94.3% on spiny dendritic shafts and 5.7% on aspiny shafts; Fig. 7B). A lower percentage of SS were established on dendritic spines ($n = 37$, 17.53%; Fig. 7E, Supplementary Table 1) and they were found more commonly on the head of the spines than on spine necks (83.8% of AS were on spine heads and 16.2% were on spines necks; Fig. 7B).

The preference of AS and SS for dendritic spines and dendritic shafts, respectively, was statistically tested. We found a consistent association ($\chi^2 = 2752.261$, $P = 0.000$) for AS and dendritic spines (receiving 99.2% AS and 0.8% SS), and for SS and dendritic shafts (receiving 31.5% AS and 68.5% SS). Regarding dendritic spines, we found that AS had a significant preference for spine heads: 99.3% of AS and only 0.7% of SS ($\chi^2 = 2873.067$, $P = 0.000$) were on spine heads, while SS had a significant preference for spine necks ($\chi^2 = 115.886$, $P = 0.000$) (with 85.7% SS established on spine necks vs. 14.3% in the case of AS). Regarding dendritic shafts, SS presented a significant preference both for spiny dendritic shafts (receiving 20.4% AS and 79.6% SS; $\chi^2 = 3039.292$, $P = 0.000$) and aspiny dendritic shafts (establishing 79.2% AS and 20.8% SS; $\chi^2 = 33.374$, $P = 0.000$) (Supplementary Tables 2 and 3).

We also determined the proportions of single and multiple synapses per spine head. The majority of synapses were single AS (99.24%). Different combinations of multiple synapses on a spine head were found as follows: 0.11% had two AS and 0.65% had one AS and one SS (Supplementary Table 4).

Cocaine-SA Group
The distribution of postsynaptic targets after cocaine-SA was similar to the saline group with only slight differences as described below (Fig. 7, Supplementary Table 1).

We observed slight differences in the distribution of postsynaptic targets after cocaine-SA in the case of AS ($\chi^2 = 7.916$, $P = 0.043$) but not for SS ($\chi^2 = 0.119$, $P = 0.989$ for SS). Specifically, following cocaine-SA, we found a slightly lower proportion of AS

on spine heads (dropping from 98.32% to 97.62%—a decrease of 0.7%, $\chi^2 = 5.786$, $P = 0.016$) and a slightly higher proportion of AS on aspiny shafts (rising from 0.79% to 1.21%: an increase of 53%, $\chi^2 = 4.268$, $P = 0.039$) (Supplementary Table 1).

No differences in the number of multiple synapses were found after cocaine-SA ($\chi^2 = 0.357$, $P = 0.550$) (Supplementary Table 4).

Synaptic Shape

Synapses were classified into four morphological categories: macular, horseshoe-shaped, perforated, and fragmented. We also refer to the group of horseshoe-shaped, perforated and fragmented synapses as synapses with complex shapes (Fig. 8A). We determined the synaptic shape of 5117 synapses (4902 AS and 215 SS) in the saline group and 4767 synapses (4589 AS and 178 SS) in the cocaine-SA group (Supplementary Table 5).

Saline Group
The four synaptic shapes were not equally present within AS and SS ($\chi^2 = 10497.767$, $P = 0.000$ and $\chi^2 = 274.167$, $P = 0.000$, respectively). The vast majority of both AS and SS had a macular shape (88.23% and 86.51%, respectively), followed by perforated synapses (7.16% and 8.84%, respectively), horseshoe-shaped synapses (4.24% and 4.65%, respectively) and fragmented synapses (0.37% and 0%, respectively, Fig. 8B; Supplementary Table 5).

We did not observe an association between the type of synapse (AS or SS) and the synaptic shape ($\chi^2 = 1.740$, $P = 0.628$).

We did not observe an association between the type of postsynaptic target and the synaptic shape for either AS ($\chi^2 = 3.149$, $P = 0.338$) or SS ($\chi^2 = 2.461$, $P = 0.277$) (Supplementary Table 6). Thus, the synaptic shape distribution was the same for axospinous and axodendritic synapses—both for AS and SS.

Cocaine-SA Group
The proportion of synaptic shapes after cocaine-SA was similar to the saline group and only slight differences were found, which we describe below (Fig. 8, Supplementary Table 5).

We observed that the distribution of synaptic shapes was different after cocaine-SA for AS ($\chi^2 = 13.916$, $P = 0.003$) and SS ($\chi^2 = 11.531$, $P = 0.005$). Specifically, for AS, we found that after cocaine-SA, macular AS were less frequently found (declining from 88.23 to 86.60—a decrease of 1.8%, $\chi^2 = 5.741$, $P = 0.017$) and fragmented AS were more frequently present (rising from 0.37 to 0.89—an increase of 140%, $\chi^2 = 10.625$, $P = 0.001$). For SS, we found that after cocaine-SA, macular SS were less frequently found (they dropped from 86.51 to 74.16—a decrease of 14%, $\chi^2 = 9.625$, $P = 0.002$) and horseshoe-shaped SS were more frequently present (rising from 4.65 to 12.36—an increase of 166%, $\chi^2 = 7.736$, $P = 0.005$) (Fig. 8, Supplementary Table 5). Regarding the postsynaptic targets, we observed that these differences were found within axospinous synapses in the case of AS ($\chi^2 = 14.812$, $P = 0.002$), and within axodendritic synapses in the case of SS ($\chi^2 = 9.210$, $P = 0.027$) (Supplementary Table 6).

The Synaptic Apposition Surface

Morphological features of the SAS were obtained with EspINA software for both AS and SS. We analyzed the SAS of 10 990 synapses in the saline group (AS = 10 561; SS = 429) and 9069 synapses in the cocaine-SA group (AS = 8756; SS = 313).
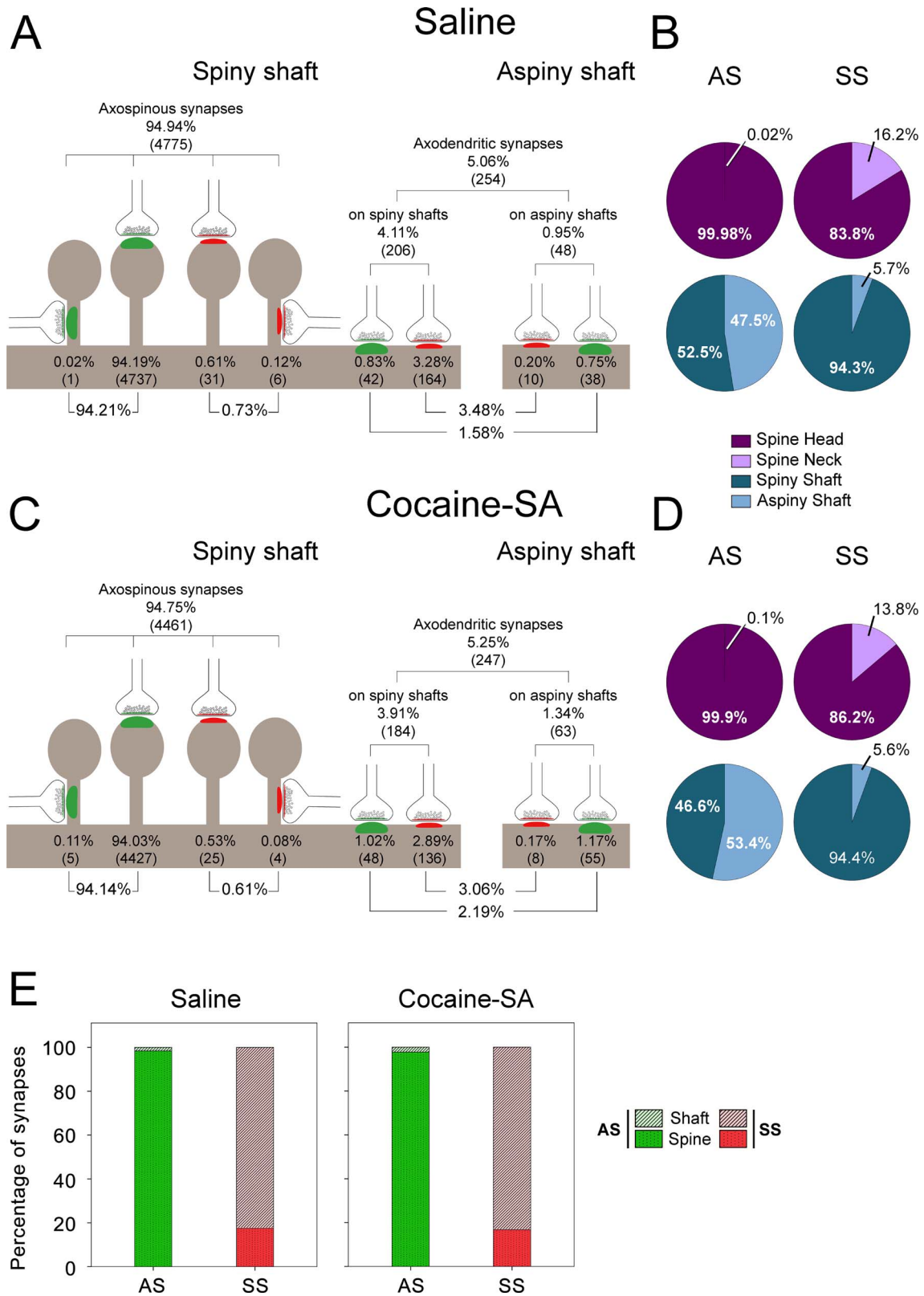
Figure 7. Distribution of synapses according to their postsynaptic targets in the *stratum radiatum* of the rat CA1 in the saline and cocaine-SA groups. (*A, C*) Percentages of axospinous (both on the head and neck of dendritic spines) and axodendritic (both on spiny and aspiny shafts) AS (green) and symmetric (SS; red) synapses in the saline and the cocaine-SA group, respectively. The numbers of each synaptic type are shown in brackets. (*B, D*) Pie charts illustrating the proportions of AS and SS according to their location as axospinous synapses (i.e., on the head or neck of the spine) or axodendritic synapses (i.e., spiny or aspiny shafts) in the saline and the cocaine-SA group, respectively. (*E*) Graph showing the percentage of axospinous and axodendritic synapses within the AS and SS populations in the saline and the cocaine-SA groups. SA: self-administration.
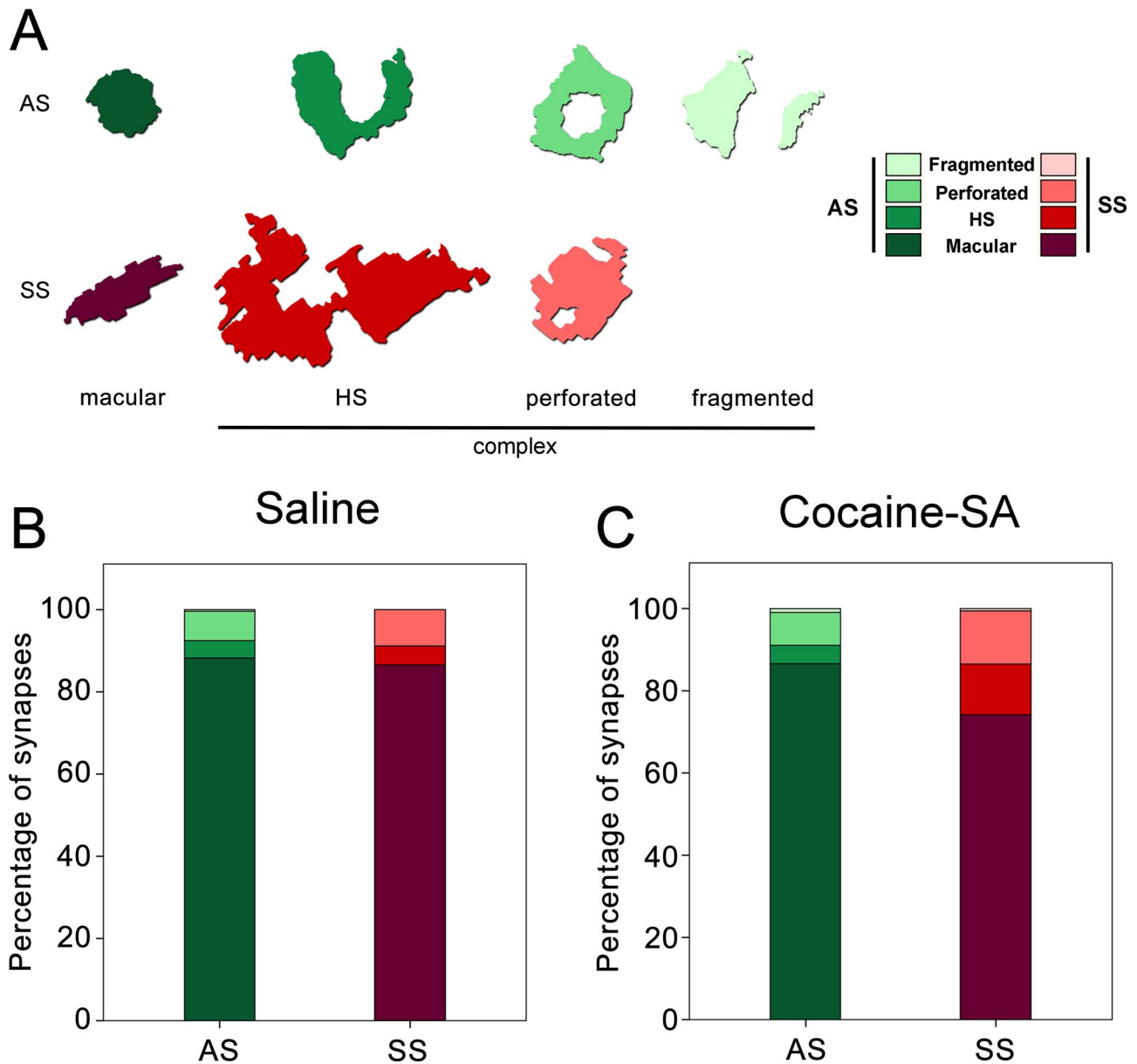
Figure 8. Proportions of synaptic shapes in the *stratum radiatum* of the rat CA1 in the saline and cocaine-SA groups. (A) Examples of the different types of synapses based on the shape of the synaptic junction: macular, horseshoe-shaped (HS), perforated, and fragmented. We also refer to nonmacular synapses as synapses with complex shapes. The upper and lower rows show examples of shapes of AS and SS synapses, respectively. (B, C) Percentages of the different types of synaptic shapes within the population of AS and SS in the saline (B) and the cocaine-SA (C) group. SA: self-administration.

Synaptic Size: SAS Area and Perimeter

Saline group. SAS areas ranged from 1990 to 318 912 nm^2 for AS, and from 3634 to 620 661 nm^2 for SS. The mean SAS area of AS (42 022 nm^2) was significantly smaller than the mean SAS area of SS (67 972 nm^2) ($t_{10} = -4.022$, $P = 0.002$) (Fig. 9A, Table 1).

Mean perimeters were larger for SS than for AS (1507 and 996 nm, respectively, $t_{10} = -5.836$, $P = 0.000$) (Table 1). There was a strong correlation between SAS area and perimeter for 1) all synapses ($R^2 = 0.936$, $P = 0.000$), 2) AS ($R^2 = 0.935$, $P = 0.000$), and 3) SS ($R^2 = 0.935$, $P = 0.000$) (Fig. 9F). Therefore, the larger the SAS area of a synapse, the more tortuous its perimeter—the SAS perimeter tends to grow longer than the perimeter of a circle (Fig. 9F).

To further characterize the size distribution of SAS, we plotted the frequency histograms of SAS areas and perimeters. For AS and SS, these frequency histograms showed a unimodal and continuous distribution with a positive skewness. The SAS area and perimeter distribution of AS statistically differed from SS ($KS = 5.927$, $P = 0.000$ for area; $KS = 7.768$, $P = 0.000$ for perimeter) and a longer right tail was observed for SS (Fig. 9B).

Additionally, we studied the synaptic size according to the postsynaptic targets (Fig. 9C,D; Supplementary Table 7). For AS, axospinous AS were the same size as axodendritic AS, while—for SS—axospinous SS were smaller than axodendritic SS. When focusing on the type of dendritic shaft, we observed that synapses on aspiny shafts were larger than synapses on
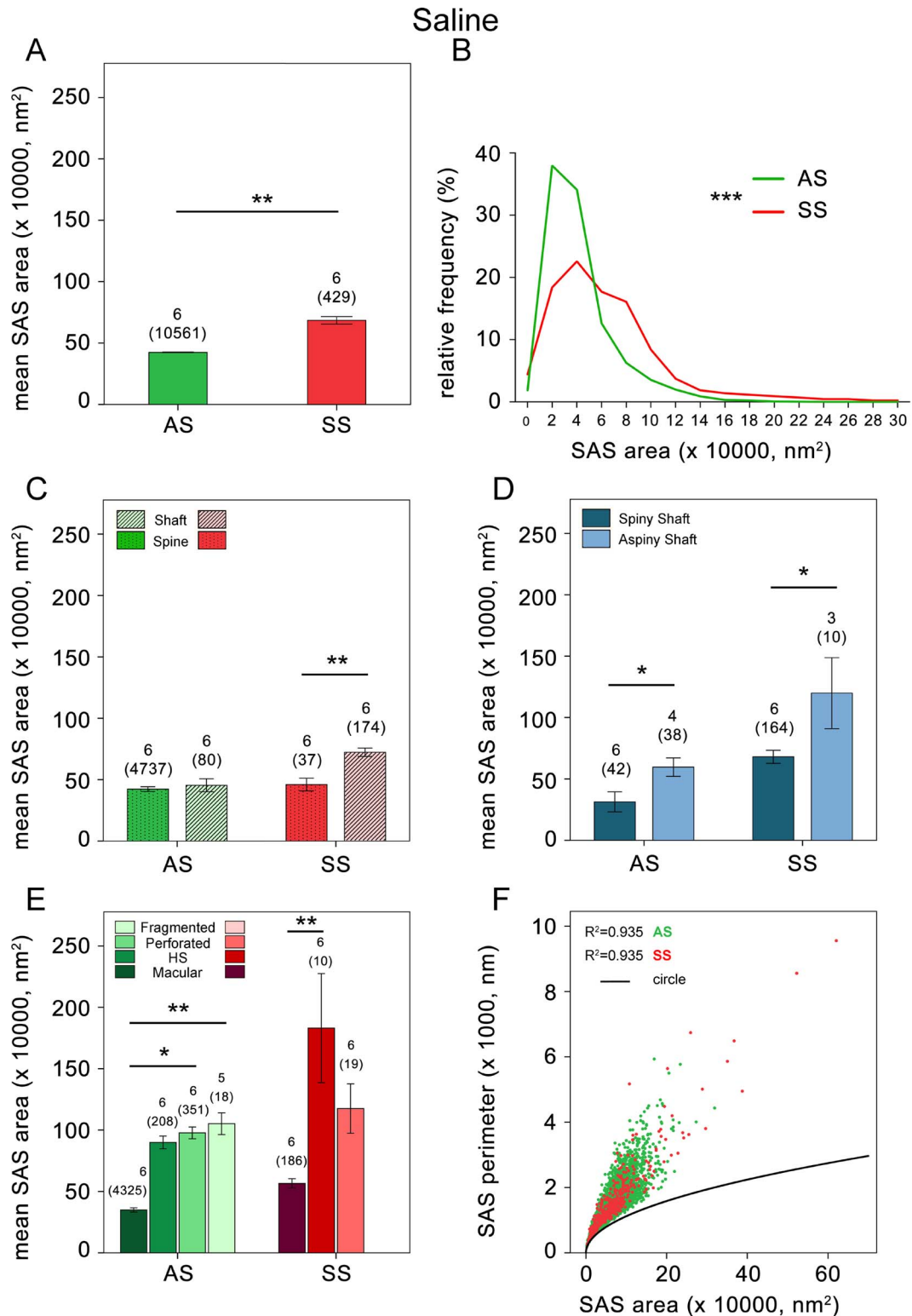
Figure 9. SAS area measurements in the *stratum radiatum* of the rat CA1 in the saline group. (A) Mean SAS area of AS (green) and symmetric (SS; red) synapses are represented (mean ± SEM). (B) Frequency distribution of SAS areas for both AS (green line) and SS (red line). (C) Mean SAS area of axospinous and axodendritic synapses are also shown for AS and SS (mean ± SEM). (D) Mean SAS area of axodendritic synapses on spiny and aspiny shafts are also shown for AS and SS (mean ± SEM). (E) Mean SAS area related to the different synaptic shapes is plotted for both AS and SS (mean ± SEM). (F) Scatter plot showing the relationship between SAS areas and perimeters. AS are represented as green dots and SS as red dots. The black trace indicates the perimeter/area relation of a circle, as a reference. There is a strong correlation between SAS area and perimeter for AS ($R^2 = 0.935$) and SS ($R^2 = 0.935$). The number of animals and the number of synapses analyzed (in brackets) is indicated. HS: horseshoe-shaped synapses; SEM: standard error of the mean. *$P < 0.05$, **$P < 0.01$, ***$P < 0.001$, see text and Supplementary Tables 7 and 8 for further information about statistical comparisons.

spiny shafts, both for AS and for SS. Finally, we analyzed the differences in the synaptic size according to the shape of the synaptic junctions (Fig. 9E; Supplementary Table 8). Macular AS were smaller than the rest of the synaptic shapes within AS, while macular SS were smaller than horseshoe-shaped SS. See Supplementary Tables 7 and 8 for information about statistical significances.

Cocaine-SA group. No differences were found in the mean SAS area or perimeter of AS and SS after cocaine-SA (AS: $t_{10} = -1.729$, $P = 0.114$ for area and $t_{10} = -1.736$, $P = 0.113$ for perimeter; SS: $t_{10} = -1.979$, $P = 0.076$ for area), with the exception of SS with larger perimeters (saline: 1507 μm; cocaine-SA: 1916 μm, $t_{10} = -2.357$, $P = 0.040$) (Table 1). In addition, we did not find significant differences after cocaine-SA in the mean SAS area or perimeter of AS and SS classified according to the postsynaptic targets or the synaptic shapes (Supplementary Tables 7 and 8).

However, when analyzing the SAS area and perimeter distribution, the cocaine-SA group showed a higher number of synapses with larger SAS area and perimeter than the saline group, both for AS (KS = 6.550, $P = 0.000$ for area; KS = 4.885, $P = 0.000$ for perimeter) and for SS (KS = 4.430, $P = 0.000$ for area; KS = 2.790, $P = 0.000$ for perimeter) (Fig. 10A,B). When focusing on the postsynaptic targets, a higher number of synapses with larger SAS area and perimeter was observed for axospinous AS after cocaine-SA (KS = 3.715, $P = 0.000$ for area; KS = 2.636, $P = 0.000$ for perimeter), while these size differences were less evident—or even nonexistent—for axodendritic AS (KS = 2.025, $P = 0.001$ for area; KS = 1.323, $P = 0.060$ for perimeter) (Fig. 10C,E). No size differences were observed for axospinous SS (KS = 0.800, $P = 0.543$ for area; KS = 0.782, $P = 0.574$), but there was a slight tendency for a higher number of synapses with larger SAS area and perimeter for axodendritic SS after cocaine-SA (KS = 1.334, $P = 0.057$ for area; KS = 1.359, $P = 0.050$ for perimeter) (Fig. 10D,F). Regarding synaptic shape, a higher number of synapses with larger SAS area and perimeter was observed within the population of macular AS after cocaine-SA (KS = 3.835, $P = 0.000$ for area; KS = 2.583, $P = 0.000$ for perimeter), while these size differences were less evident or even nonexistent for horseshoe-shaped AS (KS = 1.770, $P = 0.004$ for area; KS = 1.313, $P = 0.064$ for perimeter). No changes were observed for perforated and fragmented AS (perforated AS: KS = 1.227, $P = 0.098$ for area and KS = 0.665, $P = 0.769$ for perimeter; fragmented AS: KS = 0.585, $P = 0.884$ for area and KS = 0.867, $P = 0.439$ for perimeter) (Fig. 11A,C,E,G). For SS, only the population of perforated SS showed a slight tendency for a higher number of larger synapses after cocaine-SA (macular SS: KS = 0.852, $P = 0.462$ for area and KS = 0.936, $P = 0.346$ for perimeter; horseshoe-shaped SS: KS = 0.731, $P = 0.659$ for area and KS = 0.818, $P = 0.515$ for perimeter; perforated SS: KS = 1.484, $P = 0.024$ for area and KS = 1.144, $P = 0.146$ for perimeter) (Fig. 11B,D,F). Considering the figures for significance ($P > 0.001$ for AS), together with both the results for SAS area and perimeter distribution, we interpret that the higher proportion of larger synapses after cocaine-SA was especially evident for axospinous and macular AS, while—in the case of SS—the greater proportion of larger synapses was not so clearly associated with any specific synaptic type.

SAS Curvature

Saline group. Curvature measurements of all synapses, AS and SS, had a slightly inverse association with area ($R^2 = -0.332$, $P = 0.000$ for all synapses; $R^2 = -0.325$, $P = 0.000$ for AS; $R^2 = -0.457$, $P = 0.000$ for SS) and perimeter ($R^2 = -0.301$, $P = 0.000$ for all

synapses; $R^2 = -0.295$, $P = 0.000$ for AS; $R^2 = -0.401$, $P = 0.000$ for SS).

SS were observed to be flatter than AS (mean SAS curvature of AS: 0.0037; mean SAS curvature of SS: 0.0028) (MW = 5, $P = 0.041$) (Table 1).

The frequency histograms of SAS curvature ratios showed a positive skewness with a larger number of synapses presenting lower values, meaning a larger prevalence of flatter synapses than more curved ones for both AS and SS populations. The SAS curvature distribution of AS statistically differed from SS (KS = 2.092, $P = 0.000$) and a longer right tail was observed for AS.

With regard to the postsynaptic targets, the mean curvature ratio of axospinous and axodendritic synapses did not differ for either AS or SS (MW = 12, $P = 0.662$ for AS and MW = 21, $P = 0.699$ for SS) (Supplementary Table 7). Regarding the synaptic shape, we did not find differences in the mean curvature ratio within AS (KW = 6.677, $P = 0.083$), while differences were found within SS ($F_{2,15} = 10.466$, $P = 0.001$)—macular SS were flatter than horseshoe-shaped SS and perforated SS ($t_{15} = 4.317$, $P = 0.002$ and $t_{15} = 3.439$, $P = 0.011$, respectively) (Supplementary Table 8).

Cocaine-SA group. No differences were found in the mean curvature ratio of AS and SS after cocaine-SA ($t_{10} = 0.838$, $P = 0.422$ for AS, MW = 16, $P = 0.818$ for SS) (Table 1). Likewise, after cocaine-SA, we did not find significant differences in the mean SAS area or perimeter of AS and SS classified according to the postsynaptic targets or the synaptic shapes (Supplementary Tables 7 and 8).

Volume Fraction of Neuropil Occupied by Mitochondria

Mitochondria play a key role in energy production and calcium buffering, among many other functions, and a positive correlation between the volume fraction of mitochondria located in neuronal processes and the density of synapses has been found (Santuy et al. 2018c). Thus, we evaluated possible changes in the volume fraction of neuropil occupied by mitochondria (V_m) in the *stratum radiatum* of the CA1 field after cocaine-SA. No differences were found ($V_m = 7.31\%$ in the saline group and $V_m = 7.49\%$ in the cocaine-SA group; $t_{10} = -0.601$, $P = 0.561$) (Table 1).

Discussion

We can draw the following two main conclusions from our work:

1. In the control rats, most synapses are AS and randomly distributed. The most common synaptic type is an AS with a macular shape on a spine head. This type of synapse is also smaller than the rest of the synaptic types.
2. In the cocaine-SA rats, there are no changes in the synaptic density, the ratio of AS and SS, or in the synaptic spatial distribution. However, we observed some differences in the distribution of postsynaptic targets and synaptic shapes as well as in the synaptic size. A higher proportion of larger AS (mainly, axospinous and macular) and SS were observed. This increase in the synaptic size was accompanied by the presence of a higher proportion of synapses with more complex shapes (that have larger sizes than macular ones).

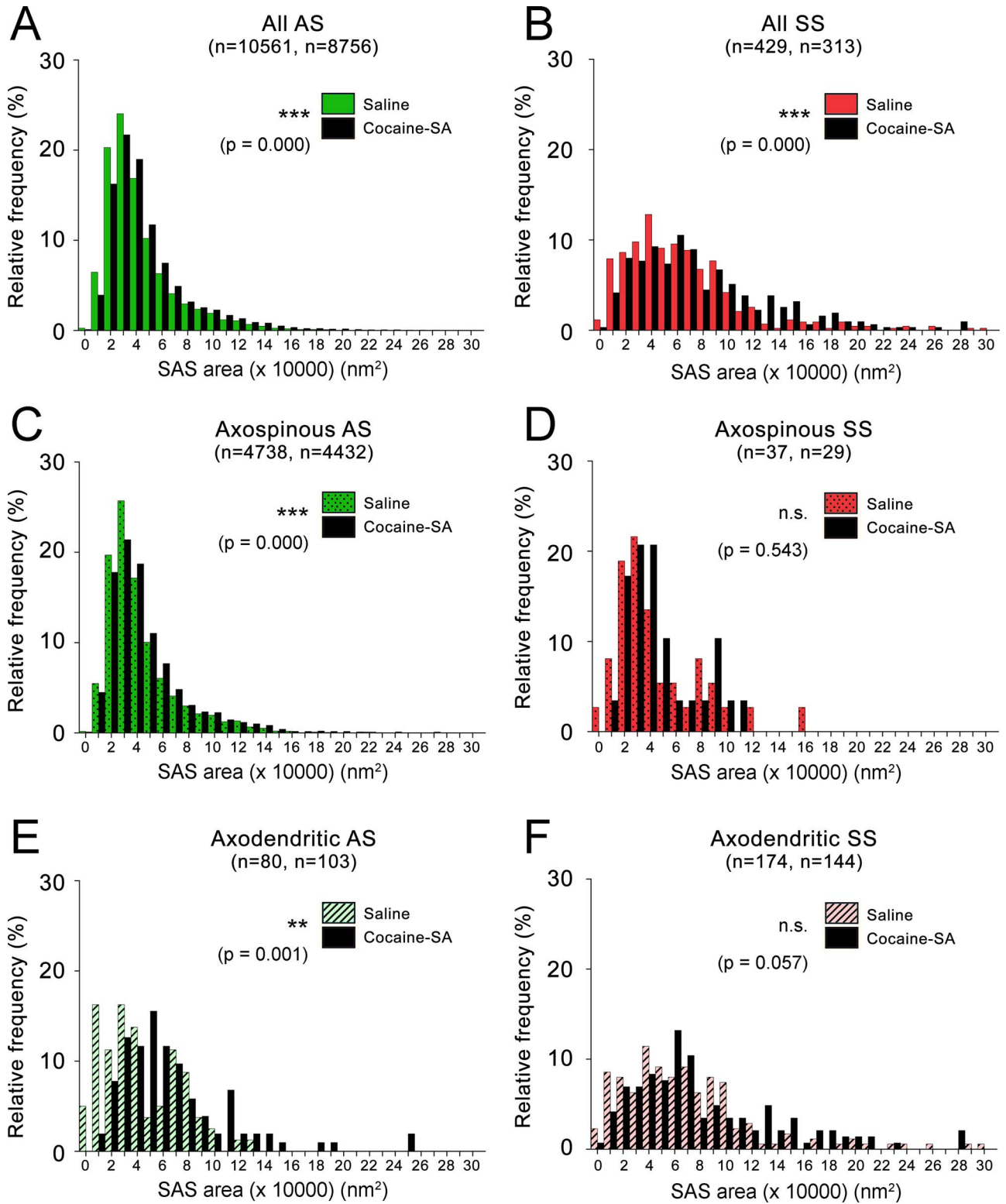A summary of the results is shown in Supplementary Figure 2 and Supplementary Table 9.

Figure 10. Frequency distribution of the SAS areas for all synapses classified according to their postsynaptic targets in the saline and cocaine-SA groups. (*A, B*) Frequency distribution of SAS areas for both AS (*A*) and SS synapses (*B*). (*C, D*) Frequency distribution of SAS areas for both axospinous AS (*C*) and axospinous SS (*D*). (*E, F*) Frequency distribution of SAS areas for both axodendritic AS (*E*) and axodendritic SS (*F*). The number of synapses in the saline and the cocaine-SA group, respectively, is indicated in brackets. SA: self-administration. **P < 0.01, ***P < 0.001, see text for further information about statistical comparisons.
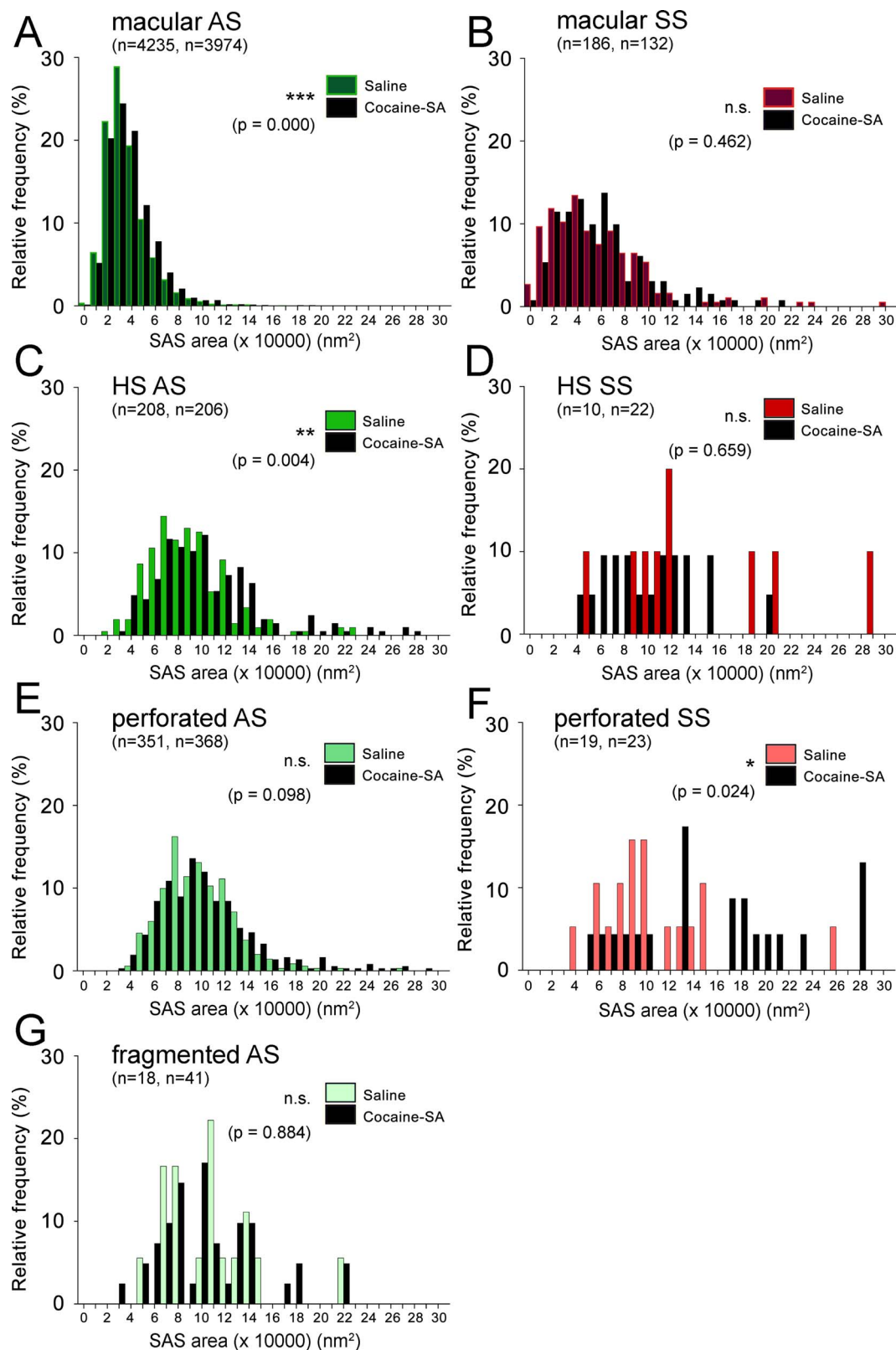
Figure 11. Frequency distribution of the SAS areas for synapses classified according to their synaptic shape in the saline and cocaine-SA groups. (*A*, *B*) Frequency distribution of SAS areas for both macular AS (*A*) and macular symmetric synapses (SS) (*B*). (*C*, *D*) Frequency distribution of SAS areas for both horseshoe-shaped AS (*C*) and horseshoe-shaped SS (*D*). (*E*, *F*) Frequency distribution of SAS areas for both perforated AS (*E*) and perforated SS (*F*). (*G*) Frequency distribution of SAS areas for fragmented AS. The number of synapses in the saline and the cocaine-SA group, respectively, is indicated in brackets. HS: horseshoe-shaped synapses; SA: self-administration. *P < 0.05, **P < 0.01, ***P < 0.001, see text for further information about statistical comparisons.

Synaptic Organization of the *Stratum Radiatum* of the Control Rat CA1 (Saline Group)

Synaptic Density, Ratio of AS and SS, and Spatial Distribution

Synaptic density. We found a synaptic density of 2.52 synapses/μm^3. Using FIB/SEM, we have previously shown that the synaptic density in the *stratum radiatum* of CA1 of the mouse is 2.36 synapses/μm^3 (Santuy et al. 2020), whereas in the *stratum radiatum* of CA1 of the human hippocampus, it is 0.67 synapses/μm^3 (Montero-Crespo et al. 2020). Thus, the synaptic density of the rat and mouse is remarkably similar but there are huge differences in synaptic density between humans and rodents. These differences—together with differences in other anatomical, genetic, molecular, and physiological features (e.g., Slomianka et al. 2011; Hawrylycz et al. 2012; Benavides-Piccione et al. 2020)—further support the notion that remarkable differences exist between the human and rodent CA1. These differences clearly need to be taken into consideration when making interpretations in translational studies comparing one species with another.

Ratio of AS and SS. It has been consistently reported that the neuropil is characterized by a much higher number of excitatory contacts compared with inhibitory synapses in different brain regions and species (Beaulieu and Colonnier 1985; Megías et al. 2001; DeFelipe et al. 2002; Mishchenko et al. 2010; Bourne and Harris 2012; Domínguez-Álvaro et al. 2018, 2019; Santuy et al. 2018a). In the present study, we found that the AS:SS ratio was 96.25:3.75. Previous results from our laboratory, using the FIB/SEM methodology, have shown that the AS:SS ratios are 98:2 and 96:4 in the *stratum radiatum* of the mouse and human CA1, respectively (Montero-Crespo et al. 2020; Santuy et al. 2020). That is, the ratio of AS and SS in the CA1 field is similar in humans and rodents.

Spatial distribution. We found that the spatial organization of synapses in the neuropil was nearly random, with slight deviations which could be explained by the presence of large apical dendrites in *stratum radiatum* that leave relatively large spaces free of synapses (see Fig. 5D). Randomly distributed synapses have been described in the neuropil of the somatosensory cortex of normal rats and the frontal and transentorhinal cortices and hippocampus of the human brain (Blazquez-Llorca et al. 2013; Merchán-Pérez et al. 2014; Domínguez-Álvaro et al. 2018; Montero-Crespo et al. 2020). This suggests that this synaptic characteristic is a widespread "rule" of the neuropil of the cerebral cortex of different species. However, slight deviations from randomness—like those we observed in the rat hippocampus—were not observed in the human hippocampus.

Postsynaptic Targets

The most abundant synaptic type was axospinous AS (94.21%), followed by axodendritic SS (3.48%) and axodendritic AS (1.58%). Axospinous SS were rarely observed (0.73%). Regarding postsynaptic preferences, most inhibitory synapses (82.47%) were on dendritic shafts, while most excitatory synapses (98.34%) were on spines (almost exclusively on the head of the spine). This preference of inhibitory and excitatory axons for dendritic shafts and dendritic spines, respectively, is also characteristic of other cortical regions and species, although variations in their percentages have been reported (Beaulieu and Colonnier 1985; Beaulieu et al. 1992; Micheva and Beaulieu 1996; Megías et al. 2001; DeFelipe et al. 2002; Mishchenko et al. 2010; Bourne and Harris 2012; Santuy et al. 2018a; Domínguez-Álvaro et al. 2019).

Regarding axospinous AS, they are especially abundant (94.21%) when compared with other brain regions in both humans and other species (Beaulieu and Colonnier 1985; Beaulieu et al. 1992; Micheva and Beaulieu 1996; Megías et al. 2001; DeFelipe et al. 2002; Mishchenko et al. 2010; Bourne and Harris 2012; Santuy et al. 2018a; Domínguez-Álvaro et al. 2019; Montero-Crespo et al. 2020). For example, in the *stratum radiatum* of the human CA1 and the somatosensory cortex of the rat, axospinous AS represent around 75% of the total synaptic population (Santuy et al. 2018a; Montero-Crespo et al. 2020) and in layer II of the human transentorhinal cortex or the *stratum lacunosum-moleculare* of the human CA1, axospinous AS are even less numerous and account for around 55% of the total synaptic population (Domínguez-Álvaro et al. 2019; Montero-Crespo et al. 2020).

The percentage of dendritic spines establishing multiple synapses was lower (0.76%) than reported in the somatosensory cortex of the rat (5.57%), the human CA1 (2.11%) or in layer II of the human transentorhinal cortex (5.52%) (Santuy et al. 2018a; Domínguez-Álvaro et al. 2019; Montero-Crespo et al. 2020).

Synaptic Shape, Synaptic Size and Curvature

Most synapses presented a simple, macular shape (around 87% for both AS and SS), in agreement with previous reports in different brain areas and species (Geinisman et al. 1986; Jones and Calverley 1991; Santuy et al. 2018b; Domínguez-Álvaro et al. 2019; Montero-Crespo et al. 2020). In our study, nonmacular synapses constituted around 13% of the total synapses. Similar results to ours have been found using FIB/SEM microscopy in the *stratum radiatum* of the human CA1 (13% nonmacular AS and 18% nonmacular SS; Montero-Crespo et al. 2020).

The shape and size of the synaptic junctions are strongly correlated with the release probability, synaptic strength, efficacy, and plasticity (Ganeshina et al. 2004a, 2004b; Holderith et al. 2012; Biederer et al. 2017). In this regard, all three types of nonmacular synapses (with more complex shapes) were larger than macular ones, as previously observed in different brain regions and species (Santuy et al. 2018b; Domínguez-Álvaro et al. 2019; Montero-Crespo et al. 2020). Although the functional significance of perforations is still unclear, perforated synapses are known to have more AMPA and NMDA receptors than macular synapses and are thought to constitute a relatively powerful population of synapses with more long-lasting memory-related functionality than their smaller, macular counterparts (Ganeshina et al. 2004a, 2004b; Spruston 2008).

Considering all synapses, inhibitory contacts were approximately 62% larger than excitatory ones—a similar trend to that observed in the rat somatosensory cortex (SS were 43% larger than AS in layers I–VI; Santuy et al. 2018b). However, this contrasted with our findings in layer II of the human transentorhinal cortex (Domínguez-Álvaro et al. 2018) and the human CA1 (Montero-Crespo et al. 2020); AS were 55% larger than SS in layer II of the transentorhinal cortex and 31% larger in the *stratum radiatum* of the CA1. Interestingly, AS are much larger (almost twice as big) in the *stratum radiatum* of the human CA1, while SS sizes in rats and humans are relatively similar (Montero-Crespo et al. 2020).

SS were observed to be flatter than AS, which were different from observations made in our previous studies in the human CA1 and transentorhinal cortex (in which no differences were found) and also different from observations in the rat somatosensory cortex (where AS were flatter than

SS) (Domínguez-Álvaro et al. 2018; Santuy et al. 2018b; Montero-Crespo et al. 2020). As previously discussed in Santuy et al. (2018b), changes in synaptic curvature have been associated with synaptic efficacy. However, unlike synaptic area, it is still not known how curvature influences synaptic functioning. Furthermore, unlike Santuy et al. (2018b) and Montero-Crespo et al. (2020), who did not find a correlation between synaptic size and curvature, we found a slight inverse correlation for synaptic size and curvature in the present study. Thus, more research is necessary to elucidate the biological relevance of this morphological parameter.

Therefore, the synaptic organization of the *stratum radiatum* of the rat CA1 shows remarkable differences compared with the same layer and region of the human hippocampus as well as compared with other brain regions and species.

Effects of Cocaine-SA on the Synaptic Organization of the Stratum Radiatum of the Rat CA1

Synaptic Density, Ratio of AS and SS, and Spatial Distribution
No significant changes were found after cocaine-SA with regard to the synaptic density, the ratio of AS and SS, or the synaptic spatial distribution. However, previous light microscopy studies from our laboratory have shown that both passive administration of cocaine (for 15 days by intraperitoneal injection) and cocaine-SA for 3 weeks increase the number of dendritic spines in the *stratum radiatum* of the CA1 field of the Lewis rat hippocampus (Del Olmo et al. 2007; Miguéns et al. 2015), which a priori could be interpreted as an increase in the number of axospinous synapses in cocaine-SA rats. This discrepancy with our results might be explained by the possibility that newly appearing dendritic spines in cocaine-SA are nonsynaptic, resulting in the increase in the spine number not being accompanied by a synaptic density increase. Thus, further studies are needed to determine if there is an increase in the proportion of nonsynaptic dendritic spines in cocaine-SA animals.

Since no differences were found in the ratio of AS and SS after cocaine-SA, the balance between excitation and inhibition does not seem to be altered in the hippocampus following cocaine-SA. However, changes in synaptic size and activity can occur independently of synaptic density or the AS:SS ratio remaining unaltered. Indeed, an imbalance between inhibitory and excitatory activity has been previously described in the ventral tegmental area (VTA) after repeated cocaine exposure (Liu et al. 2005; Bocklisch et al. 2013).

Postsynaptic Targets
The most relevant change is an increase of 53% in the proportion of axodendritic AS on aspiny shafts—that in general originate from interneurons (Ascoli et al. 2008)—after cocaine-SA (it increased from 0.79% to 1.21% of the AS population). It has been previously observed that when LTP is induced exclusively in excitatory synapses on hippocampal pyramidal neurons, the temporal fidelity of synaptic integration and action potential generation in pyramidal cells is compromised. However, when LTP also occurs at excitatory synapses on feed-forward interneurons, temporal fidelity is preserved and information processing can be maintained without degradation during memory encoding (Lamsa et al. 2005). It is possible that the increase in the proportion of AS on aspiny shafts after cocaine-SA has a relevant role in memory formation and consolidation induced by the drug.

Synaptic Shape and Synaptic Size
Regarding the synaptic shape, we observed a higher proportion of synapses with more complex shapes—particularly in the case of axospinous AS and axodendritic SS (see Supplementary Table 9). As stated above, synapses with more complex shapes are larger than macular ones; thus, the increase in the number of synapses with more complex shapes means an increase in synaptic surface.

We did not find significant differences in the mean SAS areas or perimeters, for either AS or SS after cocaine-SA (with the exception of an increase in the mean SAS perimeter of SS). However, there were differences in the frequency distribution of the SAS area and perimeter of synapses after cocaine-SA. Specifically, we observed a greater proportion of larger synapses, both AS and SS. For AS, this increase was mainly found within macular axospinous AS, while for SS it was not so clearly associated with any specific synaptic type. However, data regarding SS should be interpreted with caution since a lower number of synapses were analyzed compared with AS.

Taking both results together (regarding synaptic shape and size), cocaine-SA seems to induce an increase in the synaptic surface of axospinous AS, increasing both the proportion of synapses with more complex shapes and the size of macular synapses. In a previous study, we observed an increase in the proportion of larger dendritic spines in the Lewis rat CA1 after cocaine-SA (Selvas et al. 2017). We can therefore speculate that cocaine-SA causes an increase in synaptic activity and that this may induce the growth of macular synapses and, in some cases, lead to deep indentations and perforations appearing as the PSD becomes larger (Supplementary Fig. 2). We did not observe that the synaptic size increase was accompanied by changes in the volume fraction of the neuropil occupied by mitochondria. This is interesting because mitochondria are described as being involved in the morphogenesis and plasticity of dendritic spines and synapses (Billups and Forsythe 2002; Li et al. 2004). Thus, further studies about the possible relationship between mitochondria, synaptic organization, and cocaine effects should be performed.

Finally, several studies have analyzed the effect of cocaine-SA on the synaptic plasticity of the rat hippocampus in Lewis rats and other strains. LTP facilitation has been observed both after 3 weeks of cocaine-SA (Del Olmo et al. 2006) and following passive cocaine administration (Thompson et al. 2002). In addition, there is an impaired LTP depotentiation after 3 weeks of cocaine-SA, which seems to suggest a loss of synaptic flexibility (Miguéns et al. 2011). Thus, it is possible that changes in the synaptic plasticity (LTP facilitation and impaired LTP depotentiation) after cocaine-SA may be related. In this regard, the synapse size has been associated with different functional attributes. For example, it has been proposed that small dendritic spines (with small synapses) are preferential sites for LTP induction, while large dendritic spines (with large synapses) may represent physical long-term memory storage locations (Malik and Chattarji 2012; Fauth and Tetzlaff 2016; Lisman 2017). Our data show that synaptic size follows a unimodal and continuous distribution, so synapses cannot be divided into two groups based on their size. Therefore, if the function of the "learning or memory" synapse depends on the synaptic size, there would be no clear transition between the two types of synapses. The strengthening of the synaptic transmission after cocaine-SA (inferred from the increase in the synaptic surface) could have various functional

consequences with regard to electrically induced synaptic plasticity (Fauth and Tetzlaff 2016; Lisman 2017, see also Malik and Chattarji 2012). One possibility is that this synaptic strengthening uses part of the capacity available in CA1 neurons to generate a greater synaptic plasticity, thus preventing the subsequent facilitation of electrically-induced LTP. Alternatively, it may be that stronger synapses more effectively facilitate LTP. Based on our results and the previous electrophysiological studies already mentioned, the second hypothesis seems to be more plausible. In addition, the increase in the size of SS after cocaine-SA could be the result of a compensatory mechanism to maintain the excitatory activity within certain limits (Chevaleyre and Piskorowski 2014).

Whether the effect of cocaine on CA1 synapses depends on direct action of the drug on these synapses or the remodeling of the cortical network caused by the cocaine-SA remains unknown. Previously, by performing pharmacological experiments on hippocampal slices, we were able to show that cocaine converts early LTP to a form of LTP dependent on protein synthesis, probably through the cAMP-dependent protein kinase and extracellular signal-regulated kinase signaling cascades. We also found that metabotropic glutamate receptors are involved in this phenomenon (Fole et al. 2014). As previously discussed (in Fole et al. 2014), although it is unclear how cocaine activates glutamate receptors in the hippocampus, the functional loop between the hippocampus and VTA has been proposed to participate in long-term memory processes (Otmakhova and Lisman 1998; Luo et al. 2011). Since D2 activation seems to be involved in the long-lasting LTP induced by cocaine, we hypothesize that cocaine may mimic the entry of dopamine from the VTA to the hippocampus, modulating metabotropic glutamate receptors. Thus, drug-taking experiences become well consolidated into memory after mGluR activation. Moreover, there is a well-established connection between the amygdala and the hippocampus regarding the effects associated with cocaine-conditioned behavior. Thus, we have to consider the possibility of the basolateral amygdala influencing the hippocampus via the mGlu and dopamine receptors, as has been demonstrated by other authors (Krishnan et al. 2011).

Our results suggest that the structural reorganization of synaptic circuits plays a role in their capacity for synaptic plasticity, which may be a regulatory factor of the actions that cocaine appears to have in the potentiation of context-dependent memories during cocaine-SA. Further studies will be necessary to evaluate the long-term effects of cocaine-SA during drug withdrawal periods, to provide a more comprehensive picture of the synaptic alterations occurring in different phases of the transition from initial to established drug use.

Caveats

It should be kept in mind that some of the synaptic characteristics observed in the saline group could be due to the experimental manipulation of the animals (i.e., catheter surgery, food restriction implemented prior to the self-administration procedure or the operant learning task; Fig. 1) and these could differ from nonmanipulated animals. For example, a previous study carried out in the *stratum radiatum* of the rat CA1 reported that axospinous synapses displayed increased mean length and more frequent PSD perforations after one week of food restriction (the food intake in this group was 40% less than in the control group and animals lost around 3% of their body weight

with respect to their body weight when feeding was provided ad libitum) (Babits et al. 2016). However, the rats in this previous study were younger than in ours (they were 7 weeks old and had a body weight of around 200 g at the beginning of the experiments), and also the rat strain was different (Wistar). Furthermore, these results are based on quantitative transmission electron microscopy using random sampling from single sections, thus inferring 3D synaptic characteristics from a 2D sampling. This technology has been superseded by new 3D electron microscopy methodologies that offer more robust measurements (Merchán-Pérez et al. 2009; Morales et al. 2013). Moreover, in our experiment, food restriction was less severe since it was only applied during the initial days of the procedures (drug self-administration was carried out for 21 days and the rats were fed ad libitum during this period). Thus, the consequences of food restriction in our experiment would be expected to be very limited, if indeed there was any effect at all. In addition, both saline and cocaine self-administered rats were food restricted in the same way and followed the same procedures with the only variation being that of the saline or cocaine infusions.

Furthermore, we cannot rule out the possibility of the lever-press task training affecting the synaptic organization of the studied region. As previously discussed (in Fernández-Lamo et al. 2018), it has been suggested that the hippocampus, including its intrinsic circuit and its afferent synaptic inputs, is involved in many different functions such as object recognition (Clarke et al. 2010), spatial orientation (Moser et al. 2008), classical conditioning of eyelid responses (Berger et al. 1983; Moyer et al. 1990; McEchron and Disterhoft 1997; Gruart et al. 2006), and other forms of memory acquisition and retrieval (Bliss and Collingridge 1993; Neves et al. 2008; Wang and Morris 2010; Gruart et al. 2015). However, the hippocampus does not appear to be directly involved in the acquisition of operant conditioning tasks, except those related to the performance of appetitive and consummatory behaviors when the learning is well established, and restricted to the CA3-CA1 synapse (Jurado-Parras et al. 2013; Fernández-Lamo et al. 2018). Nevertheless, in the latter two studies, rats with chronically implanted brain electrodes were also food deprived until reaching 80–85% of their weight during the ad libitum diet before starting the operant conditioning experiment where rats learnt to press the lever following an FR-1 schedule.

It could also be argued that the catheter surgery may have had an effect on the synaptic organization. In this regard, it is important to note that we did not find differences in LTP induction or LTP depotentiation in the CA1 *stratum radiatum* between saline self-administered animals and animals that did not undergo surgery (Prakash et al. 2009; Miguéns et al. 2011). Therefore, this leads us to believe that the effect of the surgery was likely to have been very limited, if indeed it had any effect at all.

It is clear that possible methodological interactions are very difficult to avoid, which—in the present case—limits our knowledge about the synaptic organization and its functioning in physiological conditions of caged experimental animals. However, these experiments do provide an insight into the range of normal organization and functioning of the brain.

In addition, the results observed in the group that self-administered cocaine could be due not only to the pharmacological effects of cocaine, but also to some extent to the above-mentioned conditions or an interaction among them. We chose the drug consumption model of intravenous cocaine-

SA because it adds the motivational component of drug intake and it is considered the best model for simulating the pattern of consumption in humans (Spanagel 2017). However, the present work does not reveal what the effects induced by passively administered cocaine would be. Differences regarding several neurobiological and behavioral cocaine effects depending upon contingent or noncontingent drug administration have been described (Wilson et al. 1994; Dworkin et al. 1995; Hemby et al. 1997; Crespo et al. 2001, 2003; Udo et al. 2004; Lecca et al. 2007; Stefański et al. 2007; Miguéns et al. 2008; Ma et al. 2013; Radley et al. 2015; Wiskerke et al. 2016; Ploense et al. 2018), while some other works did not find any such differences (Caffino et al. 2014; Pomierny-Chamiolo et al. 2015, 2017; Terrier et al. 2016; Wright et al. 2017).

Some studies that examined the effects of contingent or noncontingent cocaine—or those that employed a food self-administration group—showed the most relevant effects when cocaine was self-administered. For example, it has been reported that cocaine produces persistent LTP in the VTA, but this is not the case for natural reward self-administration or passive cocaine infusions (Chen et al. 2008). We also previously showed, using a yoked-procedure, that excitatory amino acid transporters binding in the CA1 field of the hippocampus were decreased in cocaine self-administered animals but not in animals that received cocaine passively (Miguéns et al. 2008). In addition, GluN1 subunit expression was elevated in the hippocampus in animals that self-administered cocaine, but not in animals that received passive cocaine or self-administered food (Pomierny-Chamiolo et al. 2015). In these studies, the most relevant changes were found in cocaine self-administered animals and were not evident in passive cocaine administration or food self-administration conditions. However, it is also important to note that previous studies from our laboratory found cocaine-induced synaptic plasticity alterations in the hippocampus regardless of the drug administration method used (passive vs. self-administration; Prakash et al. 2009; Miguéns et al. 2011).

Finally, we do not know whether the observed differences in the hippocampal synaptic organization between the saline and the cocaine-SA group, which we mainly attribute to the pharmacological effect of the cocaine or an interaction between the drug and the operant learning process, could be similarly induced by a natural reward. Many studies support the view that addictive drugs usurp brain circuits used by natural rewards, especially for the dopamine-dependent reinforcing qualities of both drugs and natural rewards. However, some studies point to the hypothesis that some—but not all—sites may share signaling (Bobadilla et al. 2017). Many previous studies did not find a similar effect of self-administration of natural rewards in the synaptic structural or functional changes observed after cocaine-SA in several different brain regions, such as frontostriatal circuits (Wiskerke et al. 2016), the nucleus accumbens (Robinson et al. 2001; Gipson et al. 2013; Garcia-Keller et al. 2019), the VTA (Chen et al. 2008), and the prefrontal cortex (Robinson et al. 2001; Radley et al. 2015). Thus, taking all of this into account, it is tempting to speculate that the changes observed in the synaptic organization in the present work were due to an interaction between the pharmacological effects of cocaine and the motivational processes involved in operant learning. However, future research is needed to clarify the involvement of the pharmacological effects of cocaine and learning mechanisms in the synaptic organization of the hippocampus related to cocaine consumption.

Supplementary Material

Notes

Funding

Data Availability

The datasets generated and/or analyzed during the current study are available from the corresponding author on reasonable request.

References

Anton-Sanchez L, Bielza C, Merchán-Pérez A, Rodríguez J-R, DeFelipe J, Larrañaga P. 2014. Three-dimensional distribution of cortical synapses: a replicated point pattern-based analysis. *Front Neuroanat*. 8:85.

Arellano JI, Espinosa A, Fairén A, Yuste R, DeFelipe J. 2007. Non-synaptic dendritic spines in neocortex. *Neuroscience*. 145:464–469.

Ascoli GA, Alonso-Nanclares L, Anderson SA, Barrionuevo G, Benavides-Piccione R, Burkhalter A, Buzsáki G, Cauli B, DeFelipe J, Petilla Interneuron Nomenclature Group, et al. 2008. Petilla terminology: nomenclature of features of GABAergic interneurons of the cerebral cortex. *Nat Rev Neurosci*. 9:557–568.

Babits R, Szőke B, Sótonyi P, Rácz B. 2016. Food restriction modifies ultrastructure of hippocampal synapses: food restriction induced synaptic changes in CA1. *Hippocampus*. 26:437–444.

Baddeley A, Rubak E, Turner R. 2015. *Spatial point patterns: methodology and applications with R*. Boca Raton (FL): CRC Press.

Baddeley A, Turner R. 2005. Spatstat: an R package for analyzing spatial point patterns. *J Stat Softw*. 12:Issue6.

Ballesteros-Yáñez I, Ambrosio E, Benavides-Piccione R, Pérez J, Torres I, Miguéns M, García-Lecumberri C, DeFelipe J. 2007a. The effects of morphine self-administration on cortical pyramidal cell structure in addiction-prone Lewis rats. *Cereb Cortex*. 17:238–249.

Ballesteros-Yáñez I, Valverde O, Ledent C, Maldonado R, DeFelipe J. 2007b. Chronic cocaine treatment alters dendritic arborization in the adult motor cortex through a CB1 cannabinoid receptor-dependent mechanism. *Neuroscience*. 146:1536–1545.

Beaulieu C, Colonnier M. 1985. A laminar analysis of the number of round-asymmetrical and flat-symmetrical synapses on spines, dendritic trunks, and cell bodies in area 17 of the cat. *J Comp Neurol*. 231:180–189.

Beaulieu C, Kisvarday Z, Somogyi P, Cynader M, Cowey A. 1992. Quantitative distribution of GABA-immunopositive and -immunonegative neurons and synapses in the monkey striate cortex (area 17). *Cereb Cortex*. 2:295–309.

Beaulieu C, Somogyi P. 1990. Targets and quantitative distribution of GABAergic synapses in the visual cortex of the cat. *Eur J Neurosci*. 2:296–303.

Benavides-Piccione R, Regalado-Reyes M, Fernaud-Espinosa I, Kastanauskaite A, Tapia-González S, León-Espinosa G, Rojo C, Insausti R, Segev I, DeFelipe J. 2020. Differential structure of hippocampal CA1 pyramidal neurons in the human and mouse. *Cereb Cortex*. 30:730–752.

Berger TW, Rinaldi PC, Weisz DJ, Thompson RF. 1983. Single-unit analysis of different hippocampal cell types during classical conditioning of rabbit nictitating membrane response. *J Neurophysiol*. 50:1197–1219.

Biederer T, Kaeser PS, Blanpied TA. 2017. Transcellular Nanoalignment of synaptic function. *Neuron*. 96:680–696.

Billups B, Forsythe ID. 2002. Presynaptic mitochondrial calcium sequestration influences transmission at mammalian central synapses. *J Neurosci*. 22:5840–5847.

Blazquez-Llorca L, Merchán-Pérez Á, Rodríguez J-R, Gascón J, DeFelipe J. 2013. FIB/SEM technology and Alzheimer's disease: three-dimensional analysis of human cortical synapses. *J Alzheimers Dis*. 34:995–1013.

Bliss TVP, Collingridge GL. 1993. A synaptic model of memory: long-term potentiation in the hippocampus. *Nature*. 361:31–39.

Bobadilla A-C, Garcia-Keller C, Heinsbroek JA, Scofield MD, Chareunsouk V, Monforton C, Kalivas PW. 2017. Accumbens mechanisms for cued sucrose seeking. *Neuropsychopharmacology*. 42:2377–2386.

Bocklisch C, Pascoli V, Wong JCY, House DRC, Yvon C, de Roo M, Tan KR, Luscher C. 2013. Cocaine disinhibits dopamine neurons by potentiation of GABA transmission in the ventral tegmental area. *Science*. 341:1521–1525.

Bosch C, Masachs N, Exposito-Alonso D, Martínez A, Teixeira CM, Fernaud I, Pujadas L, Ulloa F, Comella JX, DeFelipe J, et al. 2016. Reelin regulates the maturation of dendritic spines, synaptogenesis and glial ensheathment of newborn granule cells. *Cereb Cortex*. 26:4282–4298.

Bourne JN, Harris KM. 2012. Nanoscale analysis of structural synaptic plasticity. *Curr Opin Neurobiol*. 22:372–382.

Bromer C, Bartol TM, Bowden JB, Hubbard DD, Hanka DC, Gonzalez PV, Kuwajima M, Mendenhall JM, Parker PH, Abraham WC, et al. 2018. Long-term potentiation expands information content of hippocampal dentate gyrus synapses. *Proc Natl Acad Sci USA*. 115:E2410–E2418.

Broskey NT, Daraspe J, Humbel BM, Amati F. 2013. Skeletal muscle mitochondrial and lipid droplet content assessed with standardized grid sizes for stereology. *J Appl Physiol*. 115:765–770.

Cadoni C. 2016. Fischer 344 and Lewis rat strains as a model of genetic vulnerability to drug addiction. *Front Neurosci*. 10:13.

Caffino L, Frankowska M, Giannotti G, Miszkiel J, Sadakierska-Chudy A, Racagni G, Filip M, Fumagalli F. 2014. Cocaine-induced glutamate receptor trafficking is abrogated by extinction training in the rat hippocampus. *Pharmacol Rep*. 66:198–204.

Calì C, Wawrzyniak M, Becker C, Maco B, Cantoni M, Jorstad A, Nigro B, Grillo F, De Paola V, Fua P, et al. 2018. The effects of aging on neuropil structure in mouse somatosensory cortex—a 3D electron microscopy analysis of layer 1. *PLoS One*. 13:e0198131.

Caroni P, Donato F, Muller D. 2012. Structural plasticity upon learning: regulation and functions. *Nat Rev Neurosci*. 13:478–490.

Castilla-Ortega E, Serrano A, Blanco E, Araos P, Suárez J, Pavón FJ, Rodríguez de Fonseca F, Santín LJ. 2016. A place for the hippocampus in the cocaine addiction circuit: potential roles for adult hippocampal neurogenesis. *Neurosci Biobehav Rev*. 66:15–32.

Chen BT, Bowers MS, Martin M, Hopf FW, Guillory AM, Carelli RM, Chou JK, Bonci A. 2008. Cocaine but not natural reward self-administration nor passive cocaine infusion produces persistent LTP in the VTA. *Neuron*. 59:288–297.

Chevaleyre V, Piskorowski R. 2014. Modulating excitation through plasticity at inhibitory synapses. *Front Cell Neurosci*. 8:93.

Clarke JR, Cammarota M, Gruart A, Izquierdo I, Delgado-Garcia JM. 2010. Plastic modifications induced by object recognition memory processing. *Proc Natl Acad Sci USA*. 107:2652–2657.

Crespo J, Manzanares J, Oliva J, Corchero J, Palomo T, Ambrosio E. 2001. Extinction of cocaine self-administration produces a differential time-related regulation of proenkephalin gene expression in rat brain. *Neuropsychopharmacology*. 25:185–194.

Crespo JA, Manzanares J, Oliva JM, Corchero J, García-Lecumberri C, Ambrosio E. 2003. Extinction of cocaine self-administration produces alterations in corticotropin releasing factor gene expression in the paraventricular nucleus of the hypothalamus. *Brain Res Mol Brain Res*. 117:160–167.

DeFelipe J. 2015. The dendritic spine story: an intriguing process of discovery. *Front Neuroanat*. 9:14.

DeFelipe J, Fairén A. 1993. A simple and reliable method for correlative light and electron microscopic studies. *J Histochem Cytochem*. 41:769–772.

DeFelipe J, Jones EG. 1988. A light and electron microscopic study of serotonin-immunoreactive fibers and terminals in the monkey sensory-motor cortex. *Exp Brain Res*. 71:171–182.

DeFelipe J, Marco P, Busturia I, Merchán-Pérez A. 1999. Estimation of the number of synapses in the cerebral cortex: methodological considerations. *Cereb Cortex*. 9:722–732.

DeFelipe J, Alonso-Nanclares L, Arellano JI. 2002. Microstructure of the neocortex: comparative aspects. *J Neurocytol*. 31:299–316.

Del Olmo N, Miguéns M, Higuera-Matas A, Torres I, García-Lecumberri C, Solís JM, Ambrosio E. 2006. Enhancement of hippocampal long-term potentiation induced by cocaine self-administration is maintained during the extinction of this behavior. *Brain Res*. 1116:120–126.

Del Olmo N, Higuera-Matas A, Miguéns M, García-Lecumberri C, Ambrosio E. 2007. Cocaine self-administration improves performance in a highly demanding water maze task. *Psychopharmacology (Berl)*. 195:19–25.

Descarries L, Mechawar N. 2000. Ultrastructural evidence for diffuse transmission by monoamine and acetylcholine neurons of the central nervous system. *Prog Brain Res*. 125:27–47.

Domínguez-Álvaro M, Montero-Crespo M, Blazquez-Llorca L, DeFelipe J, Alonso-Nanclares L. 2019. 3D electron microscopy study of synaptic Organization of the Normal Human Transentorhinal Cortex and its possible alterations in Alzheimer's disease. *eNeuro*. 6:ENEURO.0140-19.2019.

Domínguez-Álvaro M, Montero-Crespo M, Blazquez-Llorca L, Insausti R, DeFelipe J, Alonso-Nanclares L. 2018. Three-dimensional analysis of synapses in the transentorhinal cortex of Alzheimer's disease patients. *Acta Neuropathol Commun*. 6:20.

Dufour A, Rollenhagen A, Sätzler K, Lübke JHR. 2015. Development of synaptic boutons in layer 4 of the barrel field of the rat somatosensory cortex: a quantitative analysis. *Cereb Cortex*. 26:838–854.

Dumitriu D, Laplant Q, Grossman YS, Dias C, Janssen WG, Russo SJ, Morrison JH, Nestler EJ. 2012. Subregional, dendritic compartment, and spine subtype specificity in cocaine regulation of dendritic spines in the nucleus accumbens. *J Neurosci*. 32:6957–6966.

Dworkin SI, Co C, Smith JE. 1995. Rat brain neurotransmitter turnover rates altered during withdrawal from chronic cocaine administration. *Brain Res*. 682:116–126.

Fauth M, Tetzlaff C. 2016. Opposing effects of neuronal activity on structural plasticity. *Front Neuroanat*. 10:75.

Fernández-Lamo I, Delgado-García JM, Gruart A. 2018. When and where learning is taking place: multisynaptic changes in strength during different behaviors related to the acquisition of an operant conditioning task by behaving rats. *Cereb Cortex*. 28:1011–1023.

Fole A, González-Martín C, Huarte C, Alguacil LF, Ambrosio E, Del Olmo N. 2011. Effects of chronic cocaine administration on spatial learning and hippocampal spine density in two genetically different strains of rats. *Neurobiol Learn Mem*. 95:491–497.

Fole A, Miguens M, Higuera-Matas A, Alguacil LF, Ambrosio E, Del Olmo N. 2014. Cocaine facilitates protein synthesis-dependent LTP: the role of metabotropic glutamate receptors. *Eu Neuropsychopharmacol*. 24:621–629.

Fole A, Miguéns M, Morales L, González-Martín C, Ambrosio E, Del Olmo N. 2017. Lewis and Fischer 344 rats as a model for genetic differences in spatial learning and memory: cocaine effects. *Prog Neuropsychopharmacol Biol Psychiatry*. 76:49–57.

Gaetan C, Guyon X. 2009. *Spatial statistics and modeling*. New York (NY): Springer-Verlag.

Ganeshina O, Berry RW, Petralia RS, Nicholson DA, Geinisman Y. 2004a. Differences in the expression of AMPA and NMDA receptors between axospinous perforated and nonperforated synapses are related to the configuration and size of postsynaptic densities. *J Comp Neurol*. 468:86–95.

Ganeshina O, Berry RW, Petralia RS, Nicholson DA, Geinisman Y. 2004b. Synapses with a segmented, completely partitioned postsynaptic density express more AMPA receptors than other axospinous synaptic junctions. *Neuroscience*. 125:615–623.

Garcia-Keller C, Neuhofer D, Bobadilla A-C, Spencer S, Chioma VC, Monforton C, Kalivas PW. 2019. Extracellular matrix Signaling through β3 integrin mediates cocaine cue–induced transient synaptic plasticity and relapse. *Biol Psychiatry*. 86:377–387.

Geinisman Y, de Toledo-Morrell L, Morrell F. 1986. Aged rats need a preserved complement of perforated axospinous synapses per hippocampal neuron to maintain good spatial memory. *Brain Res*. 398:266–275.

Gipson CD, Kupchik YM, Shen H, Reissner KJ, Thomas CA, Kalivas PW. 2013. Relapse induced by cues predicting cocaine depends on rapid, transient synaptic potentiation. *Neuron*. 77:867–872.

Gruart A, Muñoz MD, Delgado-García JM. 2006. Involvement of the CA3-CA1 synapse in the acquisition of associative learning in behaving mice. *J Neurosci*. 26:1077–1087.

Gruart A, Sánchez-Campusano R, Fernández-Guizán A, Delgado-García JM. 2015. A differential and timed contribution of identified hippocampal synapses to associative learning in mice. *Cereb Cortex*. 25:2542–2555.

Gundersen HJG, Bagger P, Bendtsen TF, Evans SM, Korbo L, Marcussen N, MØLler A, Nielsen K, Nyengaard JR, Pakkenberg B, et al. 1988. The new stereological tools: Disector, fractionator, nucleator and point sampled intercepts and their use in pathological research and diagnosis. *APMIS*. 96: 857–881.

Hawrylycz MJ, Lein ES, Guillozet-Bongaarts AL, Shen EH, Ng L, Miller JA, van de Lagemaat LN, Smith KA, Ebbert A, Riley ZL, et al. 2012. An anatomically comprehensive atlas of the adult human brain transcriptome. *Nature*. 489: 391–399.

Hemby SE, Co C, Koves TR, Smith JE, Dworkin SI. 1997. Differences in extracellular dopamine concentrations in the nucleus accumbens during response-dependent and response-independent cocaine administration in the rat. *Psychopharmacology (Berl)*. 133:7–16.

Holderith N, Lorincz A, Katona G, Rózsa B, Kulik A, Watanabe M, Nusser Z. 2012. Release probability of hippocampal glutamatergic terminals scales with the size of the active zone. *Nat Neurosci*. 15:988–997.

Howard V, Reed M. 2005. *Unbiased stereology: three-dimensional measurement in microscopy*. New York (NY): Garland Science.

Illian J, Penttinen A, Stroyan H, Stroyan D. 2008. *Statistical analysis and modelling of spatial point patterns*. Hoboken, NJ: John Wiley & Sons Ltd.

Jones DG, Calverley RK. 1991. Perforated and non-perforated synapses in rat neocortex: three-dimensional reconstructions. *Brain Res*. 556:247–258.

Jurado-Parras MT, Sanchez-Campusano R, Castellanos NP, del-Pozo F, Gruart A, Delgado-Garcia JM. 2013. Differential contribution of hippocampal circuits to appetitive and consummatory behaviors during operant conditioning of behaving mice. *J Neurosci*. 33:2293–2304.

Kasthuri N, Hayworth KJ, Berger DR, Schalek RL, Conchello JA, Knowles-Barley S, Lee D, Vázquez-Reina A, Kaynig V, Jones TR, et al. 2015. Saturated reconstruction of a volume of neocortex. *Cell*. 162:648–661.

Korogod N, Petersen CC, Knott GW. 2015. Ultrastructural analysis of adult mouse neocortex comparing aldehyde perfusion with cryo fixation. *Elife*. 4:e05793.

Krishnan B, Genzer KM, Pollandt SW, Liu J, Gallagher JP, Shinnick-Gallagher P. 2011. Dopamine-induced plasticity, phospholipase D (PLD) activity and cocaine-cue behavior depend on PLD-linked metabotropic glutamate receptors in amygdala. *PLoS One*. 6:e25639.

Kulik YD, Watson DJ, Cao G, Kuwajima M, Harris KM. 2019. Structural plasticity of dendritic secretory compartments during LTP-induced synaptogenesis. *Elife*. 8:e46356.

Kutlu MG, Gould TJ. 2016. Effects of drugs of abuse on hippocampal plasticity and hippocampus-dependent learning and memory: contributions to development and maintenance of addiction. *Learn Mem*. 23:515–533.

Lamsa K, Heeroma JH, Kullmann DM. 2005. Hebbian LTP in feed-forward inhibitory interneurons and the temporal fidelity of input discrimination. *Nat Neurosci*. 8:916–924.

Lecca D, Cacciapaglia F, Valentini V, Acquas E, Di Chiara G. 2007. Differential neurochemical and behavioral adaptation to cocaine after response contingent and noncontingent exposure in the rat. *Psychopharmacology (Berl)*. 191:653–667.

Leuner B, Gould E. 2010. Structural plasticity and hippocampal function. *Annu Rev Psychol*. 61:111–140 C1-3.

Li Z, Okamoto K-I, Hayashi Y, Sheng M. 2004. The importance of dendritic mitochondria in the morphogenesis and plasticity of spines and synapses. *Cell*. 119:873–887.

Lisman J. 2017. Glutamatergic synapses are structurally and biochemically complex because of multiple plasticity processes: long-term potentiation, long-term depression, short-term potentiation and scaling. *Philos Trans R Soc Lond B Biol Sci*. 372:20160260.

Liu Q, Pu L, Poo M. 2005. Repeated cocaine exposure in vivo facilitates LTP induction in midbrain dopamine neurons. *Nature*. 437:1027–1031.

Luebke JI, Medalla M, Amatrudo JM, Weaver CM, Crimins JL, Hunt B, Hof PR, Peters A. 2015. Age-related changes to layer 3 pyramidal cells in the rhesus monkey visual cortex. *Cereb Cortex*. 25:1454–1468.

Luo AH, Tahsili-Fahadan P, Wise RA, Lupica CR, Aston-Jones G. 2011. Linking context with reward: a functional circuit from hippocampal CA3 to ventral tegmental area. *Science*. 333:353–357.

Lüscher C, Robbins TW, Everitt BJ. 2020. The transition to compulsion in addiction. *Nat Rev Neurosci*. 21:247–263.

Ma Y-Y, Henley SM, Toll J, Jentsch JD, Evans CJ, Levine MS, Cepeda C. 2013. Drug-primed reinstatement of cocaine seeking in mice: increased excitability of medium-sized spiny neurons in the nucleus accumbens. *ASN Neuro*. 5:257–271.

Malik R, Chattarji S. 2012. Enhanced intrinsic excitability and EPSP-spike coupling accompany enriched environment-induced facilitation of LTP in hippocampal CA1 pyramidal neurons. *J Neurophysiol*. 107:1366–1378.

McEchron MD, Disterhoft JF. 1997. Sequence of single neuron changes in CA1 hippocampus of rabbits during acquisition of trace eyeblink conditioned responses. *J Neurophysiol*. 78:1030–1044.

Megías M, Emri Z, Freund TF, Gulyás AI. 2001. Total number and distribution of inhibitory and excitatory synapses on hippocampal CA1 pyramidal cells. *Neuroscience*. 102:527–540.

Merchán-Pérez A, Rodriguez J-R, Alonso-Nanclares L, Schertel A, DeFelipe J. 2009. Counting synapses using FIB/SEM microscopy: a true revolution for ultrastructural volume reconstruction. *Front Neuroanat*. 3:18.

Merchán-Pérez A, Rodríguez J-R, González S, Robles V, DeFelipe J, Larrañaga P, Bielza C. 2014. Three-dimensional spatial distribution of synapses in the neocortex: a dual-beam electron microscopy study. *Cereb Cortex*. 24:1579–1588.

Micheva KD, Beaulieu C. 1996. Quantitative aspects of synaptogenesis in the rat barrel field cortex with special reference to GABA circuitry. *J Comp Neurol*. 373:340–354.

Miguéns M, Coria SM, Higuera-Matas A, Fole A, Ambrosio E, Del Olmo N. 2011. Depotentiation of hippocampal long-term potentiation depends on genetic background and is modulated by cocaine self-administration. *Neuroscience*. 187:36–42.

Miguéns M, Crespo JA, Del Olmo N, Higuera-Matas A, Montoya GL, García-Lecumberri C, Ambrosio E. 2008. Differential cocaine-induced modulation of glutamate and dopamine transporters after contingent and non-contingent administration. *Neuropharmacology*. 55:771–779.

Miguéns M, Kastanauskaite A, Coria SM, Selvas A, Ballesteros-Yañez I, DeFelipe J, Ambrosio E. 2015. The effects of cocaine self-administration on dendritic spine density in the rat hippocampus are dependent on genetic background. *Cereb Cortex*. 25:56–65.

Milton AL, Everitt BJ. 2012. The persistence of maladaptive memory: addiction, drug memories and anti-relapse treatments. *Neurosci Biobehav Rev*. 36:1119–1139.

Mironov A. 2017. Stereological morphometric grids for ImageJ. *Ultrastruct Pathol*. 41:126.

Mishchenko Y, Hu T, Spacek J, Mendenhall J, Harris KM, Chklovskii DB. 2010. Ultrastructural analysis of hippocampal neuropil from the connectomics perspective. *Neuron*. 67:1009–1020.

Montero-Crespo M, Domínguez-Álvaro M, Rondón-Carrillo P, Alonso-Nanclares L, DeFelipe J, Blázquez-Llorca L. 2020. Three-dimensional synaptic organization of the human hippocampal CA1 field. *Elife*. 9:e57013.

Morales J, Alonso-Nanclares L, Rodríguez J-R, DeFelipe J, Rodríguez A, Merchán-Pérez A. 2011. Espina: a tool for the automated segmentation and counting of synapses in large stacks of electron microscopy images. *Front Neuroanat*. 5:18.

Morales J, Rodríguez A, Rodríguez J-R, DeFelipe J, Merchán-Pérez A. 2013. Characterization and extraction of the synaptic apposition surface for synaptic geometry analysis. *Front Neuroanat*. 7:20.

Moser EI, Kropff E, Moser M-B. 2008. Place cells, grid cells, and the brain's spatial representation system. *Annu Rev Neurosci*. 31:69–89.

Motta A, Berning M, Boergens KM, Staffler B, Beining M, Loomba S, Hennig P, Wissler H, Helmstaedter M. 2019. Dense connectomic reconstruction in layer 4 of the somatosensory cortex. *Science*. 366:eaay3134.

Moyer JR, Deyo RA, Disterhoft JF. 1990. Hippocampectomy disrupts trace eye-blink conditioning in rabbits. *Behav Neurosci*. 129:523–532.

Muñoz-Cuevas FJ, Athilingam J, Piscopo D, Wilbrecht L. 2013. Cocaine-induced structural plasticity in frontal cortex correlates with conditioned place preference. *Nat Neurosci*. 16:1367–1369.

Neves G, Cooke SF, Bliss TVP. 2008. Synaptic plasticity, memory and the hippocampus: a neural network approach to causality. *Nat Rev Neurosci*. 9:65–75.

Olsen CM. 2011. Natural rewards, neuroplasticity, and non-drug addictions. *Neuropharmacology*. 61:1109–1122.

Oorschot D, Peterson D, Jones D. 1991. Neurite growth from, and neuronal survival within, cultured explants of the nervous system: a critical review of morphometric and stereological methods, and suggestions for the future. *Prog Neurobiol*. 37:525–546.

Otmakhova NA, Lisman JE. 1998. D1/D5 dopamine receptors inhibit depotentiation at CA1 synapses via cAMP-dependent mechanism. *J Neurosci*. 18:1270–1279.

Ploense KL, Vieira P, Bubalo L, Olivarria G, Carr AE, Szumlinski KK, Kippin TE. 2018. Contributions of prolonged contingent and non-contingent cocaine exposure to escalation of cocaine intake and glutamatergic gene expression. *Psychopharmacology (Berl)*. 235:1347–1359.

Pomierny-Chamiolo L, Miszkiel J, Frankowska M, Mizera J, Filip M. 2017. Neuroadaptive changes in metabotropic glutamate

mGlu2/3R expression during different phases of cocaine addiction in rats. *Pharmacol Rep.* 69:1073–1081.

Pomierny-Chamiolo L, Miszkiel J, Frankowska M, Pomierny B, Niedzielska E, Smaga I, Fumagalli F, Filip M. 2015. Withdrawal from cocaine self-administration and yoked cocaine delivery dysregulates glutamatergic mGlu5 and NMDA receptors in the rat brain. *Neurotox Res.* 27:246–258.

Prakash S, Ambrosio E, Alguacil LF, Del Olmo N. 2009. Genetic differences in hippocampal synaptic plasticity. *Neuroscience.* 161:342–346.

Radley JJ, Anderson RM, Cosme CV, Glanz RM, Miller MC, Romig-Martin SA, LaLumiere RT. 2015. The contingency of cocaine administration accounts for structural and functional medial prefrontal deficits and increased adrenocortical activation. *J Neurosci.* 35:11897–11910.

Robinson TE, Gorny G, Mitton E, Kolb B. 2001. Cocaine self-administration alters the morphology of dendrites and dendritic spines in the nucleus accumbens and neocortex. *Synapse.* 39:257–266.

Robinson TE, Kolb B. 2004. Structural plasticity associated with exposure to drugs of abuse. *Neuropharmacology.* 47:33–46.

Russo SJ, Dietz DM, Dumitriu D, Morrison JH, Malenka RC, Nestler EJ. 2010. The addicted synapse: mechanisms of synaptic and structural plasticity in nucleus accumbens. *Trends Neurosci.* 33:267–276.

Santuy A, Rodriguez JR, DeFelipe J, Merchan-Perez A. 2018a. Volume electron microscopy of the distribution of synapses in the neuropil of the juvenile rat somatosensory cortex. *Brain Struct Funct.* 223:77–90.

Santuy A, Rodríguez J-R, DeFelipe J, Merchán-Pérez A. 2018b. Study of the size and shape of synapses in the juvenile rat somatosensory cortex with 3D electron microscopy. *eNeuro.* 5:ENEURO.0377-17.2017.

Santuy A, Tomás-Roca L, Rodríguez J-R, González-Soriano J, Zhu F, Qiu Z, Grant SG, DeFelipe J, Merchan-Perez A. 2020. Estimation of the number of synapses in the hippocampus and brain-wide by volume electron microscopy and genetic labeling. *Sci Rep.* 10:14014.

Santuy A, Turégano-López M, Rodríguez JR, Alonso-Nanclares L, DeFelipe J, Merchán-Pérez A. 2018c. A quantitative study on the distribution of mitochondria in the neuropil of the juvenile rat somatosensory cortex. *Cereb Cortex.* 28:3673–3684.

Schikorski T, Stevens CF. 1997. Quantitative ultrastructural analysis of hippocampal excitatory synapses. *J Neurosci.* 17:5858–5867.

Schikorski T, Stevens CF. 1999. Quantitative fine-structural analysis of olfactory cortical synapses. *Proc Natl Acad Sci USA.* 96:4107–4112.

Selvas A, Coria SM, Kastanauskaite A, Fernaud-Espinosa I, DeFelipe J, Ambrosio E, Miguéns M. 2017. Rat-strain dependent changes of dendritic and spine morphology in the hippocampus after cocaine self-administration. *Addict Biol.* 22:78–92.

Sharpe D. 2015. Your Chi-Square test is statistically significant: now what? *Pract Assess Res Eval.* 20:Art.8.

Slomianka L, Amrein I, Knuesel I, Sørensen JC, Wolfer DP. 2011. Hippocampal pyramidal cells: the reemergence of cortical lamination. *Brain Struct Funct.* 216:301–317.

Spanagel R. 2017. Animal models of addiction. *Dialogues Clin Neurosci.* 19:247–258.

Spruston N. 2008. Neuroscience: strength in numbers. *Nature.* 452:420–421.

Stefański R, Ziółkowska B, Kuśmider M, Mierzejewski P, Wyszogrodzka E, Kołomańska P, Dziedzicka-Wasylewska M, Przewłocki R, Kostowski W. 2007. Active versus passive cocaine administration: differences in the neuroadaptive changes in the brain dopaminergic system. *Brain Res.* 1157:1–10.

Terrier J, Lüscher C, Pascoli V. 2016. Cell-type specific insertion of GluA2-lacking AMPARs with cocaine exposure leading to sensitization, cue-induced seeking, and incubation of craving. *Neuropsychopharmacology.* 41:1779–1789.

Thompson AM, Gosnell BA, Wagner JJ. 2002. Enhancement of long-term potentiation in the rat hippocampus following cocaine exposure. *Neuropharmacology.* 42:1039–1042.

Udo T, Ugalde F, DiPietro N, Eichenbaum HB, Kantak KM. 2004. Effects of persistent cocaine self-administration on amygdala-dependent and dorsal striatum-dependent learning in rats. *Psychopharmacology (Berl).* 174:237–245.

Wang S-H, Morris RGM. 2010. Hippocampal-neocortical interactions in memory formation, consolidation, and reconsolidation. *Annu Rev Psychol.* 61:49–79.

Whitlock JR. 2006. Learning induces long-term potentiation in the hippocampus. *Science.* 313:1093–1097.

Wilson JM, Nobrega José N, Corrigall WA, Coen KM, Shannak K, Kish SJ. 1994. Amygdala dopamine levels are markedly elevated after self- but not passive-administration of cocaine. *Brain Res.* 668:39–45.

Wiskerke J, Schoffelmeer ANM, De Vries TJ. 2016. Response contingency directs long-term cocaine-induced neuroplasticity in prefrontal and striatal dopamine terminals. *Eur Neuropsychopharmacol.* 26:1667–1672.

Wright AM, Zapata A, Baumann MH, Elmore JS, Hoffman AF, Lupica CR. 2017. Enduring loss of serotonergic control of orbitofrontal cortex function following contingent and noncontingent cocaine exposure. *Cereb Cortex.* 27: 5463–5476.

Yakoubi R, Rollenhagen A, von Lehe M, Miller D, Walkenfort B, Hasenberg M, Sätzler K, Lübke JH. 2019. Ultrastructural heterogeneity of layer 4 excitatory synaptic boutons in the adult human temporal lobe neocortex. *Elife.* 8:e48373.